Inorganic Chemistry

ARTICLE

pubs.acs.org/IC

Design and Development of Functionalized Cyclometalated Ruthenium Chromophores for Light-Harvesting Applications

Kiyoshi C. D. Robson,[†] Bryan D. Koivisto,[†] Aswani Yella,[‡] Barbora Sporinova,[†] Mohammad K. Nazeeruddin,[‡] Thomas Baumgartner,[†] Michael Grätzel,[‡] and Curtis P. Berlinguette*[,†]

[†]Department of Chemistry and The Institute for Sustainable Energy, Environment and Economy, University of Calgary, 2500 University Drive N.W., Calgary T2N-1N4, Canada

[‡]Laboratory of Photonics and Interfaces (LPI), Institute of Chemical Sciences and Engineering, Swiss Federal Institute of Technology (EPFL), Station 6, Lausanne CH CH-1015, Switzerland

Supporting Information

ABSTRACT: The syntheses and the electrochemical spectroscopic properties of a suite of asymmetrical *bis*tridentate cyclometalated Ru(II) complexes bearing terminal triphenylamine (TPA) substituents are reported. These complexes, which contain structural design elements common to both inorganic and organic dyes that exhibit superior power conversion efficiencies in the dye-sensitized solar cell (DSSC), are broadly formulated as $[Ru^{II}(L\text{-}2,5'\text{-thiophene-TPA-}R_1)(L\text{-}R_2)]^+$ [L = tridentate chelating ligand (e.g., 2,2′:6′,2″-terpyridine (tpy); deprotonated forms of 1,3-di(pyridin-2-yl)benzene (Hdpb) or 6-phenyl-2,2′-bipyridine (Hpbpy)); R_1 = −H, −Me, −OMe; R_2 = −H, $-CO_2Me$, $-CO_2H$]. The following structural attributes were systematically modified for the series: (i) electron-donating character of the terminal substituents (e.g., R_1 = −H, −Me, −OMe) placed *para* to the amine of the "L-2,5′-thiophene-TPA-R_1" ligand framework; (ii) electron-withdrawing character of the tridentate chelate distal to the TPA-substituted ligand (e.g., R_2 = −H, $-CO_2Me$, $-CO_2H$); and (iii) position of the organometallic bond about the Ru(II) center. UV−vis spectra reveal intense and broad absorption bands arising from a collection of metal-to-ligand charge-transfer (MLCT) and TPA-based intraligand charge-transfer (ILCT) transitions that, in certain cases, extend beyond 800 nm. Electrochemical data indicate that the oxidative behavior of the TPA and metal chelate units can be independently modulated except in cases where the anionic phenyl ring is in direct conjugation with the TPA unit. In most cases, the anionic character of the cyclometalating ligands renders a metal-based oxidation event prior to the oxidation of the TPA unit. This situation can, however, be reversed with an appropriately positioned Ru−C bond and electron-rich R_1 group. This finding is important in that this arrangement confines the highest occupied molecular orbital (HOMO) to the TPA unit rather than the metal, which is optimal for sensitizing TiO_2; indeed, a remarkably high power conversion efficiency (η) in the DSSC (i.e., 8.02%) is measured for the TPA-substituted $pbpy^-$ chelate where R_1 = −OMe. These results provide a comprehensive strategy for improving the performance of *bis*tridentate Ru sensitizers devoid of NCS^- groups for the DSSC.

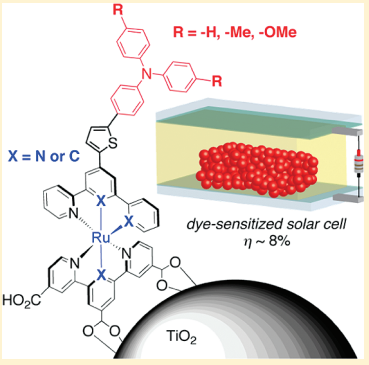

INTRODUCTION

Polypyridyl ruthenium(II) complexes are often characterized by a broad metal-to-ligand charge-transfer (MLCT) absorbance band in the visible region of the electromagnetic spectrum.[1,2] This feature, in combination with the rich luminescence behavior and redox stability in both the ground and the excited states, has driven the fundamental development of Ru(II) complexes for a wide variety of applications (e.g., artificial photosynthetic frameworks,[3−5] sensors,[6−8] and catalysis[9−12]). One particular application that has garnered a significant amount of attention is the dye-sensitized solar cell (DSSC) pioneered by O'Regan and Grätzel in 1991.[13] This study demonstrated that the sensitization of a mesoporous, wide band gap semiconductor with a Ru(II) complex is an effective means of extracting useful electrical work from incident sunlight.[14−16] With certified power conversion efficiencies (η) in excess of 11%, the DSSC currently represents the most efficient "next-generation" solar cell technology;[17,18] thus, the optimization of stable Ru(II) dyes for light-harvesting applications remains at the frontier of chemical discovery.[19]

The principal mode of sensitization for a wide band gap semiconductor (e.g., TiO_2) in the DSSC by conventional Ru(II) dyes, such as $Ru(dcbpyH_2)_2(NCS)_2$ (**N3**; $dcbpyH_2$ = 4,4′-dicarboxy-2,2′-bipyridine), relies on a light-driven MLCT transition followed by charge-injection into the anode.[15,16,20−23] The generation of higher photocurrents vis-à-vis chromophore design demands that the absorptance of the dye be appropriately matched to the solar spectrum.[21,24,25] A common strategy for achieving this goal is the replacement of up to two $-CO_2H$ groups of **N3** with conjugated and/or aliphatic substituents.[19,26] Representing a significant departure from this line of inquiry is the recent demonstration that monodentate NCS^- groups can

Received: January 4, 2011

   dx.doi.org/10.1021/ic200011m | *Inorg. Chem.* XXXX, XXX, 000–000

Chart 1. Designation of Compounds[a]

		Donor Ligand				Acceptor Ligand		
	n		-R_1	X	Y		Z	-R_2
1	2	**L1**	-H	N	N	**L8**	N	-H
2	1	**L1**	-H	N	N	**L9**	C	-H
3	1	**L2**	-H	N	C	**L10**	N	-CO_2Me
4	1	**L2**	-H	N	C	**L11**	N	-CO_2H
5	2	**L3**	-Me	N	N	**L8**	N	-H
6	1	**L3**	-Me	N	N	**L9**	C	-H
7	1	**L4**	-Me	C	N	**L8**	N	-H
8	1	**L4**	-Me	C	N	**L10**	N	-CO_2Me
9	1	**L4**	-Me	C	N	**L11**	N	-CO_2H
10	1	**L5**	-Me	N	C	**L10**	N	-CO_2Me
11	1	**L5**	-Me	N	C	**L11**	N	-CO_2H
12	2	**L6**	-OMe	N	N	**L8**	N	-H
13	1	**L6**	-OMe	N	N	**L9**	C	-H
14	1	**L7**	-OMe	N	C	**L10**	N	-CO_2Me
15	1	**L7**	-OMe	N	C	**L11**	N	-CO_2H

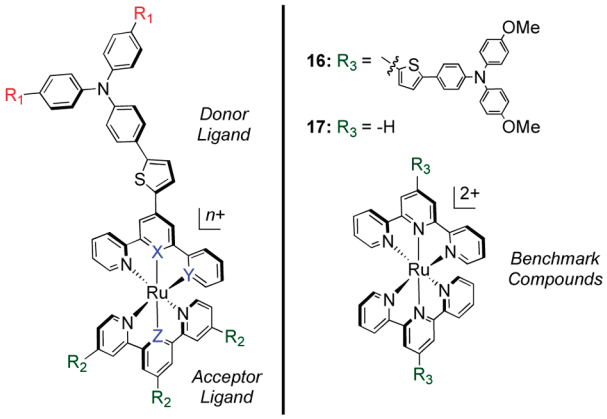

[a]Counterion = Cl^- for **2**, **6**−**7**, **13**, **16**; NO_3^- for **1**, **3**, **5**, **8**, **10**, **12**, **14**; PF_6^- for **17**; **4**, **9**, **11**, and **15** are neutral zwitterionic complexes because of the monodeprotonation of acceptor ligand. "Donor Ligand" and "Acceptor Ligand" descriptors reflect the relative position of the electron-rich TPA substituents only.

be substituted by cyclometalating ligands while preserving the light-harvesting properties. This tactic was first documented by van Koten et al., in the form of tridentate cyclometalated complexes of the general formula $[Ru^{II}(N^{\wedge}N^{\wedge}N)(N^{\wedge}N^{\wedge}C)]^{1+}$.[27] Building on this study, the Grätzel program generated a η value of 10.1% in a DSSC with the *tris*-bidentate cyclometalated complex, $[Ru(dcbpyH_2)_2(ppyF_2)]^+$ ($ppyF_2$ = 2-(2,4-difluorophenyl)pyridine).[28] This result represented a tour de force in the field on the basis that $[Ru(dcbpyH_2)_2(ppyF_2)]^+$ was the first "champion" (i.e., η > 10%) dye devoid of NCS^- groups at the time of its discovery (other examples of such champion dyes have very recently been reported[29,30]). Indeed, related Ru(II) dyes with anionic ligands have started to emerge in the literature with $\eta \sim 10\%$.[31,32]

While the utility of cyclometalated Ru complexes in photochemical applications has been independently recognized by Constable,[33−37] Sauvage,[38,39] Hammarström and Johansson,[40] and others,[41−50] the rational design of these types of complexes for sensitizing TiO_2 has not been explored to a significant extent.[27,28] A favorable feature of this class of sensitizers in the context of light-harvesting is the highest occupied molecular orbital (HOMO) being extended over the metal and the anionic portion of the cyclometalating ligand, while holding the lowest-unoccupied molecular orbital (LUMO) to the neutral polypyridyl ligands.[35,51−56] This scenario leads to a series of broad absorption bands in the visible region that arise from a suite of mixed-metal-ligand-to-ligand charge-transfer transitions, while maintaining the ground- and excited-state energy levels at appropriate positions for electron injection and regeneration in the DSSC.[55] Light absorption thus positions the excited-state electron density on the polypyridyl ligand attached to the semiconductor to enable rapid and efficient charge-injection into the TiO_2 anode.[21−23] Moreover, the replacement of the NCS^- groups with a cyclometalating ligand also offers the unique opportunity to independently tune *both* the metal-based HOMO and the ligand π^*-based LUMO.[57] Because the NCS^- ligands of Ru sensitizers are labile in practical DSSC devices,[58] chelating cyclometalating ligands also offer a promising approach for increasing the stability of Ru sensitizers.

Although we and others have shown that *polypyridyl* Ru(II) complexes bearing triphenyl-amine (TPA) substituents produce an intense absorption band in the visible region arising from multiple MLCT and ILCT transitions, the high local symmetry about the metal induces an absorption band that is too narrow for harvesting sunlight effectively.[59−62] Moreover, electron-injection into TiO_2 by polypyridyl *bis*tridentate Ru(II) derivatives can also be hampered by competing decay pathways in the absence of specifically tailored ligand modifications.[2,21,63,64] Cyclometalating ligands provide an avenue for overcoming said problems because the Ru−C σ-bond can (i) reduce the local symmetry of the metal site to generate a relatively *broad* absorption envelope; (ii) increase the energy of the LUMO to potentially enable more facile electron-injection into the TiO_2 anode; and (iii) destabilize metal-centered (MC) excited states that provide access to nonradiative pathways.[41,55] We therefore report herein a comprehensive catalogue of heteroleptic *cyclometalated* Ru(II) complexes containing an electron-rich TPA-substituted tridentate ligand opposite a tridentate chelate with, in certain cases, electron-deficient substituents capable of binding to semiconductor surfaces (Chart 1).

Inspiration for the molecular motif of **1**−**15** is drawn from the high performance of organic dyes bearing TPA units[65] (which represents the donor in the only organic dye documented to generate η > 10% in the DSSC[30]) and the enhancement in extinction coefficients when donating ligands are juxtaposed to acceptor ligands within *bis*tridentate Ru complexes.[1,2,56] The TPA unit also serves as a secondary redox-active unit that has been shown to suppress recombination between the conduction band electrons and the oxidized sensitizer in polypyridyl Ru sensitizers.[60,66−71] The 2,5-thiophene bridge between the TPA fragment and the tridentate ligand serves to circumvent steric repulsion between the adjacent aromatic six-membered rings to encourage a planar arrangement for enhanced conjugation.[59] This paper details the facile synthetic pathways to this suite of complexes, and provides a systematic evaluation of the electrochemical and photophysical response to substitution at R_1 and R_2 and the position of the organometallic bond. A comparative performance of select dye complexes is also evaluated in the

dx.doi.org/10.1021/ic200011m |*Inorg. Chem.* XXXX, XXX, 000–000

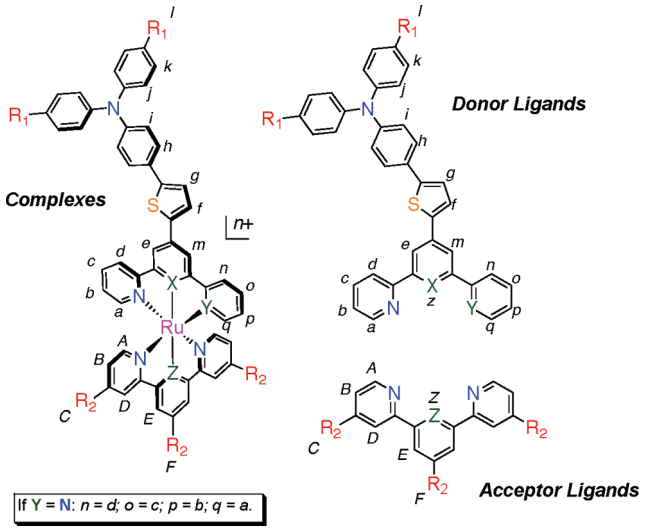

Figure 1. Labeling scheme for ^{1}H NMR signal assignments.

DSSC (η up to 8.02%) to gain insight into how to optimize this framework for light-harvesting applications.

EXPERIMENTAL SECTION

Preparation of Compounds. All reactions and manipulations were performed using solvents passed through an MBraun solvent purification system prior to use. All reagents were purchased from Aldrich and used without further purification except for $RuCl_3 \cdot 3H_2O$ (Pressure Chemical Company) and trimethyl-4,4′,4″-tricarboxylate-2,2′:6′,2″-terpyridine (**L10**; Helio Chemicals Company, Switzerland). Purification by column chromatography was carried out using silica (Silicycle: Ultrapure Flash Silica) or basic alumina (Fluka). Analytical thin-layer chromatography (TLC) was performed on aluminum-backed sheets precoated with silica 60 F254 adsorbent (0.25 mm thick; Merck, Germany) or with plastic-backed sheets precoated with basic alumina 200 F254 adsorbent (0.25 mm thick, Selecto Scientific: Georgia, U.S.A.) and visualized under UV light. Routine ^{1}H and ^{13}C NMR spectra were recorded at 400 and 100 MHz, respectively, on a Bruker AV 400 instrument at ambient temperature unless otherwise stated. Chemical shifts (δ) are reported in parts per million (ppm) from low- to high-field and referenced to residual nondeuterated solvent. Standard abbreviations indicating multiplicity are used as follows: s = singlet; d = doublet; t = triplet; m = multiplet. All proton assignments correspond to the generic molecular scheme provided in Figure 1. Organic compounds 4′-(2-thienyl)-2,2′:6′,2″-terpyridine (**P1**),[72] 2,2′-(5-(thiophen-2-yl)-1,3-phenylene)dipyridine (**P2**),[73] 6-phenyl-4-(thiophen-2-yl)-2,2′-bipyridine (**P3**),[74] 4′-(5-bromo-2-thienyl)-2,2′:6′,2″-terpyridine (**P4**),[75,76] 2-(4-diphenylaminophenyl)-4,4,5,5-tetramethyl-1,3,2-dioxaborolane (**P7**),[77] 4-methyl-*N*-(4-(4,4,5,5-tetramethyl-1,3,2-dioxaborolan-2-yl)phenyl)-*N*-*p*-tolylaniline (**P8**),[78] *N*,*N*-bis(4-methoxyphenyl)-*N*-(4-(4,4,5,5-tetramethyl-1,3,2-dioxaborolan-2-yl)phenyl)amine (**P9**),[79] 2-(3,5-dibromophenyl)-1,3-dioxolane (**P11**),[80] 4′-(5-(4-(diphenylamino)phenyl)-thiophen-2-yl)-2,2′:6′,2″-terpyridine (**L1**),[59] 1,3-bis(2-pyridyl)benzene (**L9H**),[55] 4,4′,4′-tricarboxy-2,2′:6′,2″-terpyridine (H_2tctpy; **L11** = monodeprotonated form of H_3tctpy),[81] complexes [Ru(**L1**)(tpy)]-$(Cl)_2$ (**1**)[59] and $[Ru(tpy)_2](PF_6)_2$ (**17**)[55] were prepared as previously reported.

*2,2′-(5-(5-Bromothiophen-2-yl)-1,3-phenylene)dipyridine (**P5**).* To a flask containing **P2** (0.91 g, 2.9 mmol) in tetrahydrofuran (THF, 30 mL) was added *N*-bromosuccinimide (0.57 g, 3.2 mmol). The reaction mixture was then stirred at room temperature in the dark for 12 h. The sample was preabsorbed on silica, followed by the removal of solvent in vacuo. The product was then purified by column chromatography [SiO_2: CH_2Cl_2/EtOAc 3:1; R_f = 0.50] to yield 1.10 g (96%) of the product as a white solid. ^{1}H NMR (400 MHz, $CDCl_3$): δ = 8.72 (ddd, 2H, ^3J = 4.8, ^4J = 1.8, ^5J = 1.0 Hz, H_a), 8.50 (t, 1H, ^4J = 1.6 Hz, H_z), 8.20 (d, 2H, ^4J = 1.6 Hz, H_e), 7.84 (dt, 2H, ^3J = 7.9, ^4J = 1.1 Hz, H_d), 7.77 (ddd, 2H, ^3J = 7.9, 7.4, ^4J = 1.8 Hz, H_c), 7.25 (ddd, 2H, ^3J = 7.4, 4.8, ^4J = 1.2 Hz, H_b), 7.22 (d, 1H, ^3J = 3.9 Hz, H_f), 7.04 (d, 1H, ^3J = 3.9 Hz, H_g); ^{13}C NMR (100 MHz, $CDCl_3$): δ = 156.8, 150.0, 145,7, 140.9, 137.0, 134.9, 131.1, 125.1, 124.9, 124.2, 122.8, 121.0, 112.0; HRMS (EI): m/z = 393.9959 [$(M)^+$] (calcd for $C_{20}H_{13}BrN_2S^+$: m/z = 393.9962).

*4-(5-Bromothiophen-2-yl)-6-phenyl-2,2′-bipyridine (**P6**).* A mixture of **P3** (0.900 g, 4.20 mmol) and NBS (0.748 g, 4.20 mmol) was stirred in a THF/acetic acid (2:1; 45 mL) solution at room temperature for 12 h. Following the removal of THF under reduced pressure, the suspension was neutralized with $NaHCO_3$, and the aqueous fraction was extracted with Et_2O. The organic layers were combined, dried with $MgSO_4$, and filtered. The solvent was removed in vacuo to leave a solid that was triturated with MeOH to remove residual NBS and the corresponding amide. The solid was collected by filtration, and dried under air to yield 1.20 g (73%) of the product as a white powder. ^{1}H NMR (400 MHz, $CDCl_3$): δ = 8.70 (ddd, 1H, ^3J = 4.8, ^4J = 1.8, ^5J = 1.0 Hz, H_a), 8.63 (ddd, 1H, ^3J = 8.0, ^4J = 1.0, ^5J = 1.0 Hz, H_d), 8.52 (d, 1H, ^4J = 1.6 Hz, H_e), 8.14 (d, 2H, ^3J = 7.0 Hz, H_n), 7.84 (dt, 1H, ^3J = 7.5, ^4J = 1.8 Hz, H_c), 7.81 (d, 1H, ^4J = 1.6 Hz, H_m), 7.54−7.45 (m, 3H $H_{o,p}$), 7.44 (d, 1H, ^3J = 3.9 Hz, H_f), 7.33 (ddd, 1H, ^3J = 7.5, ^3J = 4.8, ^4J = 1.0 Hz, H_b), 7.11 (d, 1H, ^3J = 3.9 Hz, H_g); ^{13}C NMR (100 MHz, $CDCl_3$): δ = 157.6, 156.7, 156.1, 149.2, 143.5, 142.5, 139.2, 137.0, 131.4, 128.9, 127.2, 125.9, 124.2, 121.6, 116.3, 115.4, 115.2, 114.3; HRMS (EI): m/z = 393.9945 [$(M)^+$] (calcd for $C_{22}H_{17}N_3O_2^+$: m/z = 393.9962).

*N,N-Diphenyl-4-(5-(6-phenyl-2,2′-bipyridin-4-yl)thiophen-2-yl)aniline (**L2H**).* **P7** (0.38 g, 1.0 mmol) and **P6** (0.36 g, 0.91 mmol) were solubilized in a THF/water solution (9:1; 130 mL) and degassed for 10 min by sparging with N_2. K_2CO_3 (0.70 g, 5.05 mmol) and $Pd(PPh_3)_4$ (80 mg, 0.07 mmol) were added, and the reaction refluxed for 18 h under N_2. The reaction mixture was cooled and poured into water. The product was extracted with ether, and the ether layer was washed with brine. The organic fractions were collected and dried with $MgSO_4$, filtered, and the solvent removed in vacuo. The resulting oil was then solubilized in CH_2Cl_2 and purified by column chromatography [SiO_2: CH_2Cl_2, R_f = 0.50] to yield a yellow/green oil. The product was then triturated with MeOH to yield 0.34 g (66%) of the product as a yellow/green solid. ^{1}H NMR (400 MHz, $CDCl_3$): δ = 8.72 (d, 1H, ^3J = 5.3 Hz, H_a), 8.65 (d, 1H, ^3J = 7.9 Hz, H_d), 8.61 (d, 1H, ^4J = 1.6 Hz, H_e), 8.18 (d, 2H, ^3J = 7.1 Hz, H_n), 7.91 (d, 1H, ^4J = 1.7 Hz, H_m), 7.83 (dt, 1H, ^3J = 7.8, ^4J = 1.6 Hz, H_c), 7.62 (d, 1H, ^3J = 3.9 Hz, H_f), 7.55−7.42 (m, 5H, H_o, H_h, H_p), 7.35−7.25 (m, 6H, H_b, H_g, H_k), 7.17−7.04 (m, 8H, H_j, H_i, H_l); ^{13}C NMR (100 MHz, $CDCl_3$): δ = 157.4, 156.5, 156.4 149.2, 148.0, 147.6, 146.0, 143.3, 140.0, 139.5, 137.0, 129.6, 129.5, 129.3, 128.9, 127.9, 127.2, 126.9, 126.8, 124.9, 124.0, 123.5 122.4, 121.7, 116.3, 115.3; HRMS (EI): m/z = 557.1930 [$(M)^+$] (calcd for $C_{38}H_{27}N_3S^+$: m/z = 557.1926).

*4-(5-(4′-(2,2′:6′,2″-Terpyridine)-thiophen-2-yl)-N,N-di-p-tolylaniline (**L3**).* To a sparged THF/water solution (9:1; 125 mL) containing **P8** (1.55 g, 3.88 mmol) and **P4** (1.38 g, 3.49 mmol) was added K_2CO_3 (2.68 g, 19.4 mmol) and $Pd(PPh_3)_4$ (314 mg, 0.27 mmol). The mixture was heated at reflux for 14 h under N_2, then cooled and poured into water. The product was extracted with diethyl ether, and the organic layer was washed with brine. The organic fractions were collected, dried with $MgSO_4$, and filtered. Removal of the solvent in vacuo left an oil that was dissolved in CH_2Cl_2 and preabsorbed on basic alumina. The solvent was removed and then purified by column chromatography [basic alumina: CH_2Cl_2, R_f = 0.48] to yield 1.68 g (74%) of the product as a bright

dx.doi.org/10.1021/ic200011m |*Inorg. Chem.* XXXX, XXX, 000–000

yellow/green solid. ^{1}H NMR (400 MHz, $CDCl_3$): δ = 8.72 (ddd, 2H, ^3J = 4.8, ^4J = 1.8, ^5J = 1.0 Hz, H_a), 8.66 (s, 2H, H_e), 8.62 (ddd, 2H, ^3J = 7.5, ^4J = 1.2, ^5J = 1.2 Hz, H_d), 7.84 (ddd, 2H, ^3J = 7.5, 7.5, ^4J = 1.8 Hz, H_c), 7.70 (d, 1H, ^3J = 3.9 Hz, H_f), 7.48 (d, 2H, ^3J = 8.8 Hz, H_h), 7.32 (ddd, 2H, ^3J = 7.4, 4.8, ^4J = 1.2 Hz, H_b), 7.23 (d, 1H, ^3J = 3.9 Hz, H_g), 7.08 (d, 4H, ^3J = 8.3 Hz, H_k), 7.04−6.98 (m, 6H, H_i, H_j), 2.32 (s, 6H, H_l); ^{13}C NMR (100 MHz, $CDCl_3$): δ = 156.3, 156.2, 149.3, 148.4, 146.5, 145.1, 143.6, 139.7, 137.0, 133.2, 130.2, 127.1, 126.7, 125.2, 125.1, 124.0, 123.2, 122.3, 121.5, 116.8, 21.1; HRMS (EI): m/z = 586.2184 [$(M)^+$] (calcd for $C_{39}H_{30}N_4S^+$: m/z = 586.2191).

*4-(5-(3,5-Di(pyridin-2-yl)phenyl)thiophen-2-yl)-N,N-di-p-tolylaniline (**L4H**).* A sparged THF/water solution (9:1; 125 mL) containing **P8** (1.25 g, 3.13 mmol) and **P5** (1.11 g, 2.82 mmol) was added K_2CO_3 (2.16 g, 15.7 mmol) and $Pd(PPh_3)_4$ (253 mg, 0.22 mmol). The reaction mixture was heated at reflux for 14 h under N_2, then cooled and poured into water. The product was extracted with diethyl ether and washed with brine, dried over $MgSO_4$, and filtered. The oil left upon removal of solvent was solubilized in CH_2Cl_2 and preabsorbed on silica. The solvent was removed, and the sample was purified by column chromatography [SiO_2: CH_2Cl_2/EtOAc, 9:1, R_f = 0.66] to yield 1.57 g (86%) of the product as a yellow solid. ^{1}H NMR (400 MHz, $CDCl_3$): δ = 8.73 (ddd, 2H, ^3J = 4.8, ^4J = 1.8, ^5J = 1.0 Hz, H_a), 8.49 (t, 1H, ^4J = 1.6 Hz, H_z), 8.31 (d, ^4J = 1.6 Hz, 2H, H_e), 7.87 (dt, 2H, ^3J = 7.9, ^4J = 1.1 Hz, H_d), 7.77 (ddd, 2H, ^3J = 7.9, 7.4, ^4J = 1.8 Hz, H_c), 7.49−7.44 (m, 3H, H_h, H_f), 7.26 (ddd, 2H, ^3J = 7.4, 4.8, ^4J = 1.2 Hz, H_b), 7.20 (d, 1H, ^3J = 3.9 Hz, H_g), 7.07 (d, 4H, ^3J = 8.2 Hz, H_k), 7.24−6.98 (m, 6H, H_i, H_j), 2.31 (s, 6H, H_l); ^{13}C NMR (100 MHz, $CDCl_3$): δ = 157.1, 149.3, 148.0, 145.2, 144.3, 142.2, 140.8, 137.0, 135.8, 133.0, 130.2, 127.6, 126.5, 125.0, 124.9, 124.7, 124.6, 123.1, 122.7, 122.6, 121.0, 21.0; HRMS (EI): m/z = 585.2242 [$(M)^+$] (calcd for $C_{40}H_{31}N_3S^+$: m/z = 585.2239).

*4-Methyl-N-(4-(5-(6-phenyl-2,2′-bipyridin-4-yl)thiophen-2-yl)-phenyl)-N-p-tolylaniline (**L5H**).* **P5**[78] (0.55 g, 1.4 mmol) and **P6** (0.49 g, 1.2 mmol) were solubilized in a THF/water solution (9:1; 130 mL) and degassed for 10 min by sparging with N_2. K_2CO_3 (0.95 g, 6.90 mmol) and $Pd(PPh_3)_4$ (115 mg, 0.10 mmol) were added, and the reaction refluxed for 18 h under N_2. The reaction mixture was cooled and poured into water. The product was extracted with ether, and the ether layer was washed with brine. The organic fractions were collected and dried with $MgSO_4$, filtered, and the solvent removed in vacuo. The resulting oil was then solubilized in CH_2Cl_2/EtOAc (9:1) and purified by column chromatography [SiO_2: CH_2Cl_2/EtOAc, 9:1, R_f = 0.53] to yield a yellow/green oil. The product was then triturated with MeOH to yield 0.75 g (quantitative) of the product as a yellow/green solid. ^{1}H NMR (400 MHz, $CDCl_3$): δ = 8.72 (ddd, 1H, ^3J = 4.7, ^4J = 1.6, ^5J = 0.8 Hz, H_a), 8.65 (d, 1H, ^3J = 7.9 Hz, H_d), 8.61 (d, 1H, ^4J = 1.6 Hz, H_e), 8.18 (d, 2H, ^3J = 7.1 Hz, H_n), 7.92 (d, 1H, ^4J = 1.6 Hz, H_m), 7.85 (dt, 1H, ^3J = 7.7, ^4J = 1.6 Hz, H_c), 7.66 (d, 1H, ^3J = 3.9 Hz, H_f), 7.55−7.42 (m, 5H, H_o, H_h, H_p), 7.33 (ddd, 1H, ^3J = 7.4, ^3J = 4.8, ^4J = 1.1 Hz, H_b), 7.24 (d, 1H, ^3J = 3.9 Hz, H_g), 7.09 (d, 4H, ^3J = 9.0 Hz, H_k), 7.02 (d, 4H, ^3J = 8.4, H_j), 7.01 (d, 2H, ^3J = 8.8, H_i); ^{13}C NMR (100 MHz, $CDCl_3$): δ = 157.5, 156.4, 156.4 149.1, 148.5, 146.5, 145.1, 143.5, 139.7, 139.6, 137.2, 133.3, 130.2, 129.4, 128.9, 127.3, 126.9, 126.8, 126.7, 125.2, 124.1, 123.2, 122.3, 121.8, 116.4, 115.4, 21.1; HRMS (EI): m/z = 585.2262 [$(M)^+$] (calcd for $C_{40}H_{31}N_3S^+$: m/z = 585.2239).

*4-(5-(4′-(2,2′:6′,2″-Terpyridine)-thiophen-2-yl)-N,N-bis(4-methoxyphenyl)aniline (**L6**).* To a sparged THF/water solution (9:1; 125 mL) containing **P9** (3.00 g, 6.96 mmol) and **P4**[75,76] (2.47 g, 6.26 mmol) was added K_2CO_3 (4.81 g, 34.8 mmol) and $Pd(PPh_3)_4$ (560 mg, 0.49 mmol). The mixture was heated at reflux for 14 h under N_2, then cooled and poured into H_2O. The product was extracted with diethyl ether and washed with brine. The organic layers were dried over $MgSO_4$ and filtered. Solvent was removed in vacuo leaving an oil that was solubilized in CH_2Cl_2 and preabsorbed on silica. The solvent was removed, and the residue was purified by column chromatography [SiO_2: CH_2Cl_2/EtOAc, 7:3; R_f = 0.50] to yield 3.1 g (72%) of the product as a bright yellow solid. ^{1}H NMR (400 MHz, $CDCl_3$): δ = 8.71 (ddd, 2H, ^3J = 4.7, ^4J = 1.8, ^5J = 1.0 Hz, H_a), 8.64 (s, 2H, H_e), 8.61 (ddd, 2H, ^3J = 8.0, ^4J = 1.0, ^5J = 1.0 Hz, H_d), 7.83 (ddd, 2H, ^3J = 7.6, 7.6, ^4J = 1.8 Hz, H_c), 7.68 (d, 1H, ^3J = 3.9 Hz, H_f), 7.45 (d, 2H, ^3J = 8.8 Hz, H_h), 7.31 (ddd, 2H, ^3J = 7.5, 4.8, ^4J = 1.2 Hz, H_b), 7.20 (d, 1H, ^3J = 3.8 Hz, H_g), 7.07 (d, 4H, ^3J = 9.0 Hz, H_k), 6.91 (d, 2H, ^3J = 9.0 Hz, H_i), 6.84 (d, 4H, ^3J = 9.0 Hz, H_j), 3.78 (s, 6H, H_l); ^{13}C NMR (100 MHz, $CDCl_3$): δ = 156.3, 156.2, 149.3, 148.9, 146.6, 143.6, 140.7, 139.5, 137.0, 127.1, 127.0, 126.7, 126.1, 124.0, 122.9, 121.5, 120.4, 116.7, 115.2, 115.0, 55.7, 21.1; HRMS (EI): m/z = 618.2092 [$(M)^+$] (calcd for $C_{39}H_{30}N_4O_2S^+$: m/z = 618.2089).

*4-Methoxy-N-(4-methoxyphenyl)-N-(4-(5-(6-phenyl-2,2′-bipyridin-4-yl)thiophen-2-yl)phenyl)aniline (**L7H**).* To a sparged THF/H_2O (7:3; 50 mL) solution containing **P4** (0.456 g, 1.16 mmol) and **P9** (0.600 g, 0.139 mmol) was added K_2CO_3 (1.23 g, 11.6 mmol) and $Pd(PPh_3)_4$ (70 mg, 0.06 mmol), and set to reflux for 14 h under N_2 (reaction completion was verified by TLC). The residue that was left upon removal of solvent was purified by column chromatography [SiO_2: CH_2Cl_2/EtOAc, 6:4; R_f = 0.86] to yield 0.585 g (82%) of the product as a yellow powder. ^{1}H NMR (400 MHz, $CDCl_3$): δ = 8.71 (ddd, 1H, ^3J = 4.7, ^4J = 1.6, ^5J = 0.8 Hz, H_a), 8.65 (d, 1H, ^3J = 7.9 Hz, H_d), 8.59 (d, 1H, ^4J = 1.6 Hz, H_e), 8.18 (d, 2H, ^3J = 7.1 Hz, H_n), 7.90 (d, 1H, ^4J = 1.6 Hz, H_m), 7.83 (dt, 1H, ^3J = 7.7, ^4J = 1.6 Hz, H_c), 7.63 (d, 1H, ^3J = 3.9 Hz, H_f), 7.52 (t, 2H, ^3J = 7.1 Hz, H_o), 7.46−7.43 ($H_{h,p}$), 7.31 (ddd, 1H, ^3J = 7.4, ^3J = 4.8, ^4J = 1.1 Hz, H_b), 7.21 (d, 1H, ^3J = 3.9 Hz, H_g), 7.08 (d, 4H, ^3J = 9.0 Hz, H_k), 6.93 (d, 2H, ^3J = 6.8 Hz, H_i), 6.85 (d, 4H, ^3J = 9.0 Hz, H_j); ^{13}C NMR (100 MHz, $CDCl_3$): δ = 157.3, 156.5, 156.4, 156.3, 149.2, 148.9, 146.5, 143.4, 139.5, 139.4, 137.0, 129.3, 128.9, 127.2, 127.0, 126.8, 126.6, 125.9, 124.0, 122.9, 121.6, 120.3, 116.2, 115.3, 115.1, 115.0, 55.6; HRMS (EI): m/z = 617.2131 [$(M)^+$] (calcd for $C_{40}H_{31}N_3O_2S^+$: m/z = 617.2137).

General Synthetic Procedure for 2, 6, 7, and 13. Unless otherwise stated, a 60 mL MeOH/H_2O/THF (5:1:1 *v/v/v*) solution containing $RuCl_3$(**L#**) (0.40 mmol), **L#** (0.40 mmol), and 0.5 mL of *N*-ethylmorpholine was stirred at reflux for 14 h under N_2. Following the removal of solvent in vacuo, the crude mixture was preabsorbed on silica and purified by column chromatography to yield a dark colored solid. The solid was solubilized in CH_2Cl_2 and filtered to remove residual SiO_2, and then drawn out of solution with diethyl ether to yield the product as the Cl^- salt.

*[Ru(L1)(L9)]Cl (**2**).* Chromatographic conditions [SiO_2: Acetone/MeOH LiCl, 4:1; R_f = 0.73]. Yield (150 mg, 42%) as a deep red microcrystalline solid. ^{1}H NMR (400 MHz, CD_3OD): δ = 9.15 (s, 2H, H_e), 8.74 (d, 2H, ^3J = 7.9 Hz, H_d), 8.32 (d, 2H, ^3J = 7.7 Hz, H_E), 8.19 (d, 2H, ^3J = 8.1 Hz, H_D), 8.17 (d, 1H, ^3J = 3.8 Hz, H_f), 7.75 (dt, 2H, ^3J = 9.0, ^4J = 1.5 Hz, H_c), 7.72 (d, 2H, ^3J = 8.7 Hz, H_h), 7.64 (dt, 2H, ^3J = 8.9, ^4J = 1.5 Hz, H_c), 7.57 (d, 1H, ^3J = 3.9 Hz, H_g), 7.34 (m, 4H, $H_{a,A}$), 7.18 (d, 2H, ^3J = 5.3 Hz, H_l), 7.16−7.08 (m, 8H, $H_{j,k}$), 7.03 (t, 2H, ^3J = 6.1 Hz, H_b), 6.71 (t, 2H, ^3J = 7.2 Hz, H_B); LRMS(ESI): m/z = 891.7 [$(M - Cl)^+$] (calcd for $C_{53}H_{37}N_6RuS^+$: m/z = 891.1). Anal. Calcd for $C_{53}H_{37}N_6RuSCl\cdot 2H_2O$: C, 66.14; H, 4.29; N, 8.73. Found: C, 65.87; H, 4.29; N, 8.63.

*Ru(L2)(L10)]NO_3 (**3**).* **L2H** (0.27 g, 0.49 mmol) was suspended in MeOH:H_2O:THF (5:1:1, *v/v*, 420 mL), and Ru(**L10**)Cl_3 (0.30 g, 0.49 mmol) and *N*-ethylmorpholine (0.5 mL) were added and refluxed for 16 h. $AgNO_3$ (0.25 g, 1.5 mmol) was added and was allowed to stir an additional 1.5 h at reflux. The mixture was cooled, preabsorbed on to silica, and the solvent was removed in vacuo. The product was purified by column chromatography [SiO_2; CH_2Cl_2/MeOH, 9:1; R_f = 0.77] to yield 391 mg (71.1%) of the product as a reddish-brown fine solid. ^{1}H NMR (400 MHz, $CDCl_3$): δ = 9.14 (s, 2H, H_E), 8.96 (d, 1H, ^3J = 7.7 Hz, H_d), 8.94 (s, 1H, H_e), 8.94 (s, 2H, H_D), 8.21 (s, 1H, H_m), 8.17(d, 1H, ^3J = 3.7 Hz, H_f), 7.93 (t, 1H, ^3J = 7.6 Hz, H_c), 7.71 (d, 2H,

dx.doi.org/10.1021/ic200011m |*Inorg. Chem.* XXXX, XXX, 000–000

^3J = 6.1 Hz, H_A), 7.62 (dd, 2H, ^3J = 6.2, ^4J = 1.1 Hz, H_B), 7.53 (d, 2H, ^3J = 8.8 Hz, H_h), 7.38 (d, 1H, ^3J = 3.7 Hz, H_g), 7.28−7.24 (m, 5H, H_b, H_k), 7.20 (d, 1H, ^3J = 6.8 Hz, H_n), 7.12 (d, 4H, ^3J = 9.0 Hz, H_j), 7.09−7.02 (m, 6H, H_l, H_j), 6.75 (t, 1H, ^3J = 7.3 Hz, H_o), 6.47 (t, 1H, ^3J = 7.3 Hz, H_p), 5.35 (d, 1H, ^3J = 7.6 Hz, H_q), 4.17 (s, 3H, H_F), 3.93 (s, 6H, H_C); HRMS (ESI): m/z = 1065.2017 [$(M)^+$] (calcd for $C_{59}H_{43}N_6O_6RuS^+$: m/z = 1065.2008). Anal. Calcd for $C_{59}H_{43}N_7O_9RuS\cdot 2H_2O$: C, 60.92; H, 4.07; N, 8.33. Found: C, 60.80; H, 4.08; N, 7.95.

[Ru(L2)(L11H$_2$)] (***4***). A flask containing **3** (140 mg, 0.12 mmol) was suspended in 25 mL of a DMF:NEt$_3$:H$_2$O (3:1:1 *v*/*v*) mixed solvent system and refluxed under N_2 overnight. The solvent was then removed in vacuo, and the crude mixture was triturated with CH_2Cl_2 to yield 117 mg (95.6%) of the product as a very dark brown fine solid. ^{1}H NMR (400 MHz, DMSO): δ = 9.46 (s, 2H, H_E), 9.21 (s, 2H, H_D), 9.02 (d, 1H, ^3J = 8.3 Hz, H_d), 8.99 (s, 1H, H_e), 8.64 (s, 1H, H_m), 8.37 (d, 1H, ^3J = 3.9 Hz, H_f), 8.09 (d, 1H, ^3J = 7.8 Hz, H_n), 8.00 (t, 1H, ^3J = 7.5 Hz, H_c), 7.77−7.68 (m, 5H, H_A,H_h,H_g), 7.58 (d, 2H, ^3J = 6.2 Hz, H_B), 7.47 (d, 1H, ^3J = 5.2 Hz, H_a), 7.38−7.34 (m, 5H, H_b, H_k), 7.15−7.05 (m, 8H, H_b, H_k), 6.72 (t, 1H, ^3J = 7.3 Hz, H_o), 6.43 (t, 1H, ^3J = 7.3 Hz, H_p), 5.45 (d, 1H, ^3J = 7.6 Hz, H_q); HRMS (ESI): m/z = 1023.1528 [$(M)^+$] (calcd for $C_{56}H_{37}N_6O_6RuS^+$: m/z = 1023.1539). Anal. Calcd for $C_{56}H_{37}N_6O_6RuS\cdot 3H_2O$: C, 62.44; H, 4.02; N, 7.80. Found: C, 62.41; H, 4.16; N, 7.95.

[Ru(L3)(L8)](NO$_3$)$_2$ (***5***). Chromatographic conditions: [SiO_2: acetone/MeOH/H_2O, 3:1:1; R_f = 0.47]; yield = 200 mg (50%) as a deep red microcrystalline solid. ^{1}H NMR (400 MHz, CD_3OD): δ = 9.16 (s, 2H, H_e), 8.95 (d, 2H, ^3J = 8.2 Hz, H_E), 8.88 (d, 2H, ^3J = 8.0 Hz, H_D), 8.70 (d, 2H, ^3J = 8.0 Hz, H_d), 8.47 (t, 1H, ^3J = 8.1 Hz, H_F), 8.28 (d, 1H, ^3J = 3.8 Hz, H_f), 8.05−7.95 (m, 4H, H_C, H_c), 7.67 (d, 2H, ^3J = 8.7 Hz, H_h), 7.57 (d, 2H, ^3J = 5.5 Hz, H_A), 7.55 (d, 1H, ^3J = 3.8 Hz, H_g), 7.44 (d, 2H, ^3J = 5.5 Hz, H_a), 7.30−7.23 (m, 4H, H_B, H_b), 7.15 (d, 4H, ^3J = 8.2 Hz, H_k), 7.05−6.95 (m, 6H, H_i, H_j), 2.33 (s, 6H, H_l); LRMS (ESI): m/z = 460.6 [$(M - 2Cl)^{2+}$] (calcd for $C_{54}H_{41}N_7RuS^{+}$: m/z = 460.6). Anal. Calcd for $C_{54}H_{41}N_9O_6RuS\cdot 3H_2O$: C, 59.01; H, 4.31; N, 11.47. Found: C, 58.74; H, 4.04; N, 11.09.

[Ru(L3)(L9)]Cl (***6***). Chromatographic conditions: [SiO_2: CH_2Cl_2/MeOH, 9:1; R_f = 0.49]; yield = 190 mg (49%) as a deep red microcrystalline solid. ^{1}H NMR (400 MHz, CD_3OD): δ = 9.13 (s, 2H, H_e), 8.72 (d, 2H, ^3J = 8.1 Hz, H_d), 8.29 (d, 2H, ^3J = 7.7, Hz, H_E), 8.20−8.14 (m, 3H, H_D, H_f), 7.73 (t, 2H, ^3J = 7.5 Hz, H_c), 7.65 (d, 2H, ^3J = 8.6 Hz, H_h), 7.61 (t, 2H, ^3J = 7.5 Hz, H_C), 7.52 (d, 1H, ^3J = 3.7 Hz, H_g), 7.44 (t, 1H, ^3J = 7.7 Hz, H_F), 7.17 (d, 2H, ^3J = 5.6 Hz, H_a), 7.14 (d, 4H, ^3J = 8.1 Hz, H_k), 7.10 (d, 2H, ^3J = 5.6 Hz, H_A), 7.04−6.96 (m, 8H, H_j, H_i, H_b), 6.92 (t, 2H, ^3J = 6.0 Hz, H_B), 2.33 (s, 6H, H_l); LRMS (ESI): m/z = 919.0 [$(M - Cl)^+$] (calcd for $C_{55}H_{41}N_6RuS^+$: m/z = 919.0). Anal. Calcd for $C_{55}H_{41}ClN_6RuS\cdot 2CH_2Cl_2$: C, 60.89; H, 4.03; N, 7.47. Found: C, 60.52; H, 3.74; N, 7.39.

[Ru(L4)(L8)]Cl (***7***). Chromatographic conditions: [SiO_2: acetone/MeOH, 9:1); R_f = 0.79]; yield = 290 mg (62%) as a deep red microcrystalline solid. ^{1}H NMR (400 MHz, CD_3OD): δ = 8.88 (d, 2H, ^3J = 8.2 Hz, H_E), 8.55 (ddd, 2H, ^3J = 7.6, ^4J = 1.5, ^5J = 1.0 Hz, H_D), 8.53 (s, 2H, H_e), 8.30 (t, 2H, ^3J = 8.1 Hz, H_F), 8.24 (ddd, 2H, ^3J = 8.0, ^4J = 1.5, ^5J = 1.0 Hz, H_d), 7.68 (ddd, 2H, ^3J = 7.6, 7.6, ^4J = 1.5 Hz, H_C), 7.61 (ddd, 2H, ^3J = 7.6, 7.6, ^4J = 1.5 Hz, H_c), 7.59 (d, 1H, ^3J = 3.8 Hz, H_f), 7.50 (d, 2H, ^3J = 8.8 Hz, H_h), 7.30 (d, 1H, ^3J = 3.7 Hz, H_g), 7.17 (ddd, 2H, ^3J = 7.5, ^4J = 1.5, ^5J = 1.0 Hz, H_A), 7.06 (d, 4H, ^3J = 8.6 Hz, H_k), 7.04 (ddd, 2H, ^3J = 7.5, ^4J = 1.5, ^5J = 1.0 Hz, H_a), 6.93 (d, 4H, ^3J = 8.3 Hz, H_j), 6.92 (d, 2H, ^3J = 8.5 Hz, H_i), 6.90 (ddd, 2H, ^3J = 7.5, 7.4, ^5J = 1.5 Hz, H_B), 6.69 (ddd, 2H, ^3J = 7.5, 7.4, ^5J = 1.5 Hz, H_b), 2.67 (s, 6H; H_l); LRMS (ESI): m/z = 919.0 [$(M - Cl)^+$] (calcd for $C_{55}H_{41}N_6RuS^+$: m/z = 919.0). Anal. Calcd for $C_{55}H_{41}ClN_6RuS\cdot CH_2Cl_2$: C, 64.71; H, 4.17; N, 8.08. Found: C, 64.46; H, 4.03; N, 7.76.

[Ru(L4)(L10)]NO$_3$ (***8***). $AgNO_3$ (0.8 mmol) was required as well as an additional 2 h of heating at reflux. The solution was filtered while hot, and the solvent removed under reduced pressure. Chromatographic conditions: [SiO_2: CH_2Cl_2/MeOH 9:1; R_f = 0.63]; yield = 105 mg (22%) as a deep green microcrystalline solid. ^{1}H NMR (400 MHz, $CDCl_3$): δ = 9.43 (s, 2H, H_E), 9.02 (s, 2H, H_D), 8.40 (s, 2H, H_e), 8.10 (d, 2H, ^3J = 7.5 Hz, H_d), 7.60 (dt, 2H, ^3J = 7.5, ^4J = 1.5 Hz, H_c), 7.54−7.43 (m, 8H, H_a, H_f, H_h, H_A), 7.28 (d, 1H, ^3J = 3.7 Hz, H_g), 7.11−7.01 (m, 10H, H_k, H_j, H_i), 6.79 (dd, 2H, ^3J = 7.5, ^4J = 1.5 Hz, H_B), 6.69 (dt, 2H, ^3J = 7.5, 7.5, ^4J = 1.5 Hz, H_b), 4.22 (s, 3H, H_F), 3.94 (s, 6H, H_C), 2.31 (s, 6H, H_l); HRMS (ESI): m/z = 1093.2313 [$(M - NO_3)^+$] (calcd for $C_{61}H_{47}N_6O_6RuS^+$: m/z = 1093.2321). Anal. Calcd for $C_{61}H_{47}N_7O_9RuS\cdot H_2O$: C, 62.45; H, 4.21; N, 8.36. Found: C, 62.09; H, 4.27; N, 8.15.

[Ru(L4)(L11H$_2$)] (***9***). Compound **8** (160 mg, 0.14 mmol) was dissolved in a DMF/H_2O/NEt_3 (3:1:1; 25 mL) solution and refluxed overnight. The solvent was removed in vacuo, and the product was washed with Et_2O, hexanes, and CH_2Cl_2, respectively, to yield 130 mg (87%) of the zwitterionic product as a brown powder. ^{1}H NMR as $^+NBu_4$ salt (400 MHz, CD_3OD): δ = 9.35 (s, 2H, H_E), 8.96 (s, 2H, H_D), 8.55 (s, 2H, H_e), 8.26 (d, 2H, ^3J = 7.5 Hz, H_d), 7.62 (t, 2H, ^3J = 7.5 Hz, H_c), 7.53 (d, 2H, ^3J = 6.0 Hz, H_A), 7.35 (d, 2H, ^3J = 5.8 Hz, H_a), 7.33 (d, 1H, ^3J = 4.0 Hz, H_g), 7.23 (d, 1H, ^3J = 4.0 Hz, H_f), 7.22 (d, 2H, ^3J = 8.8 Hz, H_h), 7.08−7.02 (m, 6H, H_B, H_k), 6.96−6.90 (m, 6H, H_i, H_j), 6.70 (t, 2H, ^3J = 7.5 Hz, H_b); HRMS (ESI): m/z = 1083.1720 [$(M)^+$] (calcd for $C_{58}H_{41}N_6O_8RuS^+$: m/z = 1083.1745). Anal. Calcd for $C_{58}H_{40}N_6O_8RuS\cdot 2H_2O$: C, 62.30; H, 3.97; N, 7.52. Found: C, 62.72; H, 3.88; N, 7.61.

[Ru(L5)(L10)]NO$_3$ (***10***). To a MeOH:H_2O:THF (5:1:1, *v*/*v*, 420 mL) suspension containing **L5H** was added Ru(**L10**)Cl_3 and *N*-ethylmorpholine (0.5 mL) followed by a 16-h reflux. $AgNO_3$ was then added to the reaction flask and left to stir for an additional 1.5-h reflux. The mixture was cooled, preabsorbed on to silica, and the solvent was removed in vacuo. The product was purified by column chromatography [SiO_2: CH_2Cl_2/MeOH. 9:1, R_f = 0.49] to yield 470 mg (68%) of the product as a reddish-brown fine solid. ^{1}H NMR (400 MHz, DMSO): δ = 9.59 (s, 2H, H_E), 9.31 (s, 2H, H_D), 9.05 (d, 1H, ^3J = 8.3 Hz, H_d), 9.01 (s, 1H, H_e), 8.67 (s, 1H, H_m), 8.38 (d, 1H, ^3J = 3.9 Hz, H_f), 8.13 (d, 1H, ^3J = 7.8 Hz, H_n), 8.04 (t, 1H, ^3J = 7.5 Hz, H_c), 7.83 (d, 2H, ^3J = 6.2 Hz, H_A), 7.74−7.67 (m, 3H, H_h, H_g), 7.64 (dd, 2H, ^3J = 6.1, ^4J = 1.2 Hz, H_B), 7.45 (d, 1H, ^3J = 5.2 Hz, H_a), 7.20−7.13 (m, 5H, H_b, H_k), 7.01 (d, 4H, ^3J = 9.0 Hz, H_j), 6.99 (d, 2H, ^3J = 8.7 Hz, H_i), 6.75 (t, 1H, ^3J = 7.3 Hz, H_o), 6.47 (t, 1H, ^3J = 7.3 Hz, H_p), 5.38 (d, 1H, ^3J = 7.6 Hz, H_q), 4.14 (s, 3H, H_F), 3.89 (s, 6H, H_C), 2.30 (s, 6H, H_l); HRMS (ESI): m/z = 1093.2333 [$(M)^+$] (calcd for $C_{61}H_{47}N_6O_6RuS^+$: m/z = 1093.2321). Anal. Calcd for $C_{61}H_{47}N_7O_9RuS\cdot 3H_2O$: C, 60.59; H, 4.42; N, 8.11. Found: C, 60.23; H, 4.16; N, 7.75.

[Ru(L5)(L11H$_2$)] (***11***). A flask containing **10** (100 mg, 0.087 mmol) was suspended in 25 mL of a DMF:NEt$_3$:H$_2$O (3:1:1 *v*/*v*) mixed solvent system and refluxed under N_2 overnight. The solvent was then removed in vacuo, and the crude mixture was triturated with CH_2Cl_2 to yield 82 mg (82%) of the product as a very dark brown fine solid. ^{1}H NMR (400 MHz, DMSO): δ = 9.46 (s, 2H, H_E), 9.21 (s, 2H, H_D), 9.02 (d, 1H, ^3J = 8.3 Hz, H_d), 8.99 (s, 1H, H_e), 8.64 (s, 1H, H_m), 8.36 (d, 1H, ^3J = 3.9 Hz, H_f), 8.10 (d, 1H, ^3J = 7.8 Hz, H_n), 8.01 (t, 1H, ^3J = 7.5 Hz, H_c), 7.73−7.67 (m, 5H, H_A,H_h,H_g), 7.59 (d, 2H, ^3J = 6.2 Hz, H_B), 7.47 (d, 1H, ^3J = 5.2 Hz, H_a), 7.20−7.13 (m, 5H, H_b, H_k), 7.01 (d, 4H, ^3J = 9.0 Hz, H_j), 6.99 (d, 2H, ^3J = 8.7 Hz, H_i), 6.73 (t, 1H, ^3J = 7.3 Hz, H_o), 6.44 (t, 1H, ^3J = 7.3 Hz, H_p), 5.43 (d, 1H, ^3J = 7.6 Hz, H_q), 2.30 (s, 6H, H_l); HRMS (ESI): m/z = 1051.1844 [$(M)^+$] (calcd for $C_{58}H_{41}N_6O_6RuS^+$: m/z = 1051.1852). Anal. Calcd for $C_{58}H_{41}N_6O_6RuS\cdot 4H_2O$: C, 58.18; H, 4.17; N, 8.27. Found: C, 58.17; H, 3.82; N, 7.93.

[Ru(L6)(L8)](NO$_3$)$_2$ (***12***). $AgNO_3$ (0.8 mmol) was required as well as an additional 2 h of heating at reflux. The solution was filtered while hot and the solvent removed under reduced pressure. Chromatographic

dx.doi.org/10.1021/ic200011m |*Inorg. Chem.* XXXX, XXX, 000–000

conditions: [SiO_2: acetone/MeOH/H_2O, 3:1:1; R_f = 0.43]; yield = 280 mg (69%) as a deep red microcrystalline solid. ^{1}H NMR (400 MHz, CD_3OD): δ = 9.15 (s, 2H, H_e), 8.96 (d, 2H, ^3J = 8.2 Hz, H_E), 8.88 (d, 2H, ^3J = 8.0 Hz, H_d), 8.70 (d, 2H, ^3J = 8.0 Hz, H_D), 8.47 (t, 1H, ^3J = 8.2 Hz, H_F), 8.27 (d, 1H, ^3J = 3.9 Hz, H_f), 8.24−7.95 (m, 4H, H_a, H_C), 7.60 (d, 2H, ^3J = 8.8 Hz, H_h), 7.57 (dd, 2H, ^3J = 5.6, ^4J = 1.0 Hz, H_a), 7.49 (d, 1H, ^3J = 3.9 Hz, H_g), 7.44 (dd, 2H, ^3J = 5.6, ^4J = 1.0 Hz, H_A), 7.30−7.22 (m, 4H, H_B, H_b), 7.07 (d, 4H, ^3J = 9.0 Hz, H_k), 6.92 (d, 4H, ^3J = 9.0 Hz, H_j), 6.89 (d, 2H, ^3J = 8.8 Hz, H_i), 3.79 (s, 6H, H_l); LRMS (ESI): m/z = 476.5 [$(M - 2NO_3)^{2+}$] (calcd for $C_{54}H_{41}N_7O_2RuS^{2+}$: m/z = 476.5). Anal. Calcd for $C_{54}H_{41}N_9O_8RuS\cdot 2H_2O$: C, 58.27; H, 4.07; N, 11.32. Found: C, 58.01; H, 4.16; N, 11.12.

[Ru(L6)(L9)]Cl (**13**). Chromatographic conditions: [SiO_2: CH_2Cl_2/MeOH, 9:1; R_f = 0.56]; yield = 450 mg (42%) as a deep red microcrystalline solid. ^{1}H NMR (400 MHz, CD_3OD): δ = 9.08 (s, 2H, H_e), 8.69 (d, 2H, ^3J = 8.0 Hz, H_d), 8.28 (d, 2H, ^3J = 7.6 Hz, H_E), 8.18 (d, 2H, ^3J = 8.0 Hz, H_D), 8.14 (d, 1H, ^3J = 3.9 Hz, H_f), 7.73 (ddd, 2H, ^3J = 8.0, 8.0, ^4J = 1.5 Hz, H_c), 7.61 (ddd, 2H, ^3J = 8.0, 8.0, ^4J = 1.5 Hz, H_C), 7.59 (d, 2H, ^3J = 8.8 Hz, H_h), 7.47 (d, 1H, ^3J = 3.9 Hz, H_g), 7.46 (t, 1H, ^3J = 7.6 Hz, H_F), 7.16 (d, 2H, ^3J = 6.0 Hz, H_a), 7.09 (d, 2H, ^3J = 6.0 Hz, H_A), 7.07 (d, 4H, ^3J = 9.0 Hz, H_k), 6.98 (ddd, 2H, ^3J = 7.6, 7.6, ^4J = 1.2 Hz, H_b), 6.91 (d, 4H, ^3J = 9.0 Hz, H_j), 6.89 (d, 2H, ^3J = 8.9 Hz, H_i), 6.68 (ddd, 2H, ^3J = 7.6, 7.6, ^4J = 1.2 Hz, H_B), 3.79 (s, 6H, H_l); LRMS (ESI): m/z = 951.2 [$(M - Cl)^+$] (calcd for $C_{55}H_{41}N_6O_2RuS^+$: m/z = 951.2). Anal. Calcd for $C_{55}H_{41}ClN_6O_2RuS\cdot 2H_2O$: C, 64.80; H, 4.44; N, 8.22. Found: C, 65.16; H, 4.61; N, 8.07.

[Ru(L7)(L10)]NO_3 (**14**). To a MeOH/H_2O/THF (5:1:1, 420 mL) solution containing **L7H** was added Ru(**L10**)Cl_3 and *N*-ethylmorpholine (0.5 mL). Following an 18 h-reflux, $AgNO_3$ was added and then left to reflux for an additional 2 h. The solution was filtered hot. The solvent was removed from the sample by rotary evaporation, followed by purification by column chromatography [SiO_2: CH_2Cl_2/MeOH, 9:1; R_f = 0.29] to yield 266 mg (69%) of the product as a dark red solid. ^{1}H NMR (400 MHz, DMSO): δ = 9.59 (s, 2H, H_E), 9.29 (s, 2H, H_D), 9.04 (d, 1H, ^3J = 8.3 Hz, H_d), 8.99 (s, 1H, H_e), 8.66 (s, 1H, H_m), 8.35 (d, 1H, ^3J = 3.9 Hz, H_f), 8.12 (d, 1H, ^3J = 7.8 Hz, H_n), 8.03 (t, 1H, ^3J = 7.5 Hz, H_c), 7.81 (d, 2H, ^3J = 6.2 Hz, H_A), 7.67−7.65 (m, 5H, H_B, H_h, H_g), 7.45 (d, 1H, ^3J = 5.2 Hz, H_a), 7.17−7.11 (m, 5H, $H_{b,k}$), 6.98 (d, 4H, ^3J = 9.0 Hz, H_j), 6.87 (d, 2H, ^3J = 8.7 Hz, H_i), 6.75 (t, 1H, ^3J = 7.3 Hz, H_o), 6.46 (t, 1H, ^3J = 7.3 Hz, H_p), 5.37 (d, 1H, ^3J = 7.6 Hz, H_q), 4.14 (s, 3H, H_F), 3.89 (s, 6H, H_C), 3.77 (s, 6H, H_l); HRMS (MALDI-TOF): m/z = 1125.2396 [$(M)^+$] (calcd for $C_{61}H_{47}N_6O_8RuS^+$: m/z = 1125.2214). Anal. Calcd for $C_{61}H_{47}N_7O_{11}RuS\cdot 1H_2O$: C, 60.74; H, 4.10; N, 7.58. Found: C, 61.07; H, 4.29; N, 7.58.

[Ru(L7)(L11)] (**15**). Compound **14** (200 mg, 0.17 mmol) was dissolved in a DMF/H_2O/NEt_3 (3:1:1; 25 mL) solution and refluxed overnight. The solvent was then removed under reduced pressure, and the resultant solid was washed successively with Et_2O, hexane, CH_2Cl_2 to yield 180 mg (91%) of the zwitterionic product as a as a deep black microcrystalline solid. ^{1}H NMR (400 MHz, DMSO): δ = 9.45 (s, 2H, H_E), 9.20 (s, 2H, H_D), 8.99 (d, 1H, ^3J = 8.3 Hz, H_d), 8.94 (s, 1H, H_e), 8.60 (s, 1H, H_m), 8.33 (d, 1H, ^3J = 2.8 Hz, H_f), 8.07 (d, 1H, ^3J = 7.8 Hz, H_n), 7.98 (t, 1H, ^3J = 7.7 Hz, H_c), 7.66−7.64 (m, 5H, H_B, H_h, H_g), 7.55 (d, 1H, ^3J = 5.8 Hz, H_A), 7.46 (d, 1H, ^3J = 5.0 Hz, H_a), 7.12−7.10 (m, 5H, H_b, H_k), 6.97 (d, 4H, ^3J = 8.0 Hz, H_j), 6.86 (d, 2H, ^3J = 8.0 Hz, H_i), 6.70 (t, 1H, ^3J = 7.4 Hz, H_o), 6.41 (t, 1H, ^3J = 7.1 Hz, H_p), 5.45 (d, 1H, ^3J = 7.4 Hz, H_q), 3.77 (S, 6H, H_l); HRMS (MALDI-TOF): m/z = 1083.1720 [$(M)^+$] (calcd for $C_{58}H_{41}N_6O_8RuS^+$: m/z = 1083.1745). Anal. Calcd for $C_{58}H_{40}N_6O_8RuS\cdot 2H_2O$: C, 62.30; H, 3.97; N, 7.52. Found: C, 62.72; H, 3.88; N, 7.61.

[Ru(L6)$_2$](Cl)$_2$ (**16**). This compound was isolated as a red powder byproduct during the preparation of **13**. Chromatographic conditions: [SiO_2: CH_2Cl_2/MeOH, 9:1; R_f = 0.40]; yield = 80 mg (29%). ^{1}H NMR (400 MHz, CD_3OD): δ = 9.16 (s, 4H, H_e), 8.88 (d, 4H, ^3J = 7.5 Hz, H_d), 8.27 (d, 2H, ^3J = 3.9 Hz, H_f), 8.02 (dt, 4H, ^3J = 7.5, ^4J = 1.5 Hz, H_c), 7.64 (d, 4H, ^3J = 8.8 Hz, H_h), 7.56 (dd, 4H, ^3J = 5.6, ^4J = 1.0 Hz, H_a), 7.53 (d, 2H, ^3J = 3.9 Hz, H_g), 7.28 (dt, 4H, ^3J = 7.5, 7.5, ^4J = 1.5 Hz, H_b), 7.10 (d, 4H, ^3J = 9.0, Hz, H_k), 6.93 (d, 4H, ^3J = 9.0 Hz, H_j), 6.91 (d, 4H, ^3J = 8.8 Hz, H_i), 3.81 (s, 12H, H_l); LRMS (ESI): m/z = 669.7 [$(M - 2Cl)^{2+}$] (calcd for $C_{78}H_{60}N_8O_4RuS_2^{2+}$: m/z = 669.6). Anal. Calcd for $C_{78}H_{60}Cl_2N_8O_7RuS_2\cdot 4H_2O$: C, 63.23; H, 4.63; N, 7.56. Found: C, 63.21; H, 4.63; N, 7.45.

Physical Methods. Elemental analysis (EA), electrospray ionization mass spectrometry (ESI-MS), matrix-assisted laser desorption/ionization mass spectrometry (MALDI-TOF), and electron impact (EI) mass spectrometry data were collected at the Chemistry Instrumentation Facility of the University of Calgary. Electrochemical measurements were performed under anaerobic conditions with a Princeton Applied Research VersaStat 3 potentiostat using dry solvents, Pt working and counter electrodes, a Ag pseudoreference electrode, and 0.1 M NBu_4BF_4 supporting electrolyte. Electronic spectroscopic data were collected on MeOH solutions using a Cary 5000 UV−vis spectrophotometer (Varian). Steady-state emission spectra were obtained at room temperature using an Edinburgh Instruments FLS920 Spectrometer equipped with a Xe900 450W steady state xenon arc lamp, TMS300-X excitation monochromator, TMS300-M emission monochromator, Hamamatsu R2658P PMT detector and corrected for detector response. Lifetime measurements were obtained at room temperature using an Edinburgh Instruments FLS920 Spectrometer equipped with Fianium SC400 Super Continuum White Light Source and Hamamatsu R3809U-50 Multi Channel Plate detector; data were analyzed with Edinburgh Instruments F900 software. Curve fitting of the data was performed using a nonlinear least-squares procedure in the F900 software.

DFT Calculations. Density functional theory (DFT) calculations were carried out using B3LYP[82−85] (Becke's three-parameter exchange functional (B3) and the Lee−Yang−Parr correlation functional (LYP)) and the LanL2DZ basis set[86−89] with an effective core potential for Ru, C, N, and S and a 6-31G* basis set was used for H atoms. All geometries were fully optimized in the ground states. Time-dependent density functional theory (TD-DFT) calculations were performed using this methodology, and the first 60 singlet−singlet transitions were calculated. The calculations by first-principles method were used for obtaining the accurate excitation energies and oscillator strengths. TD-DFT calculations were conducted with a PCM solvation model (MeOH). All calculations were carried out with the Gaussian 03W software package.[90]

Cell Fabrication. TiO_2 electrodes of 15 μm thickness were deposited onto transparent conducting glass (Nippon Sheet Glass, which has been coated with a fluorine-doped stannic oxide layer, sheet resistance of 8−10 Ω/cm^2) over which a scattering layer of ~4.5 μm thickness containing 400-nm anatase TiO_2 particles (CCIC, HPW-400) was screen-printed. These films were gradually sintered at 500 °C for 30 min. The heated electrodes were impregnated with a 0.05 M titanium tetrachloride solution in a water-saturated desiccator for 30 min at 70 °C and then washed with distilled water. The electrodes were heated again at 500 °C for 30 min and then left to cool to 50 °C before dipping them into the dye solution (3×10^{-4} M in ethanol). The electrodes were dipped in the dye solution for >18 h at 22 °C. The dye sensitized TiO_2 electrodes were assembled with Pt counter electrodes by heating with a hot-melt Surlyn film (Surlyn 1702, 25 μm thickness, DuPont) as a spacer in between the electrodes.

For photovoltaic measurements of the DSSCs, the irradiation source was a 450 W xenon light source (Osram XBO 450, Germany) with a filter (Schott 113), whose power was regulated to the AM 1.5G solar standard by using a reference Si photodiode equipped with a color matched filter (KG-3, Schott) to reduce the mismatch in the region of 350−750 nm between the simulated light and AM 1.5G to less than 4%. To reduce scattered light from the edge of the glass electrodes of the dyed TiO_2 layer, a light-shading black mask was used to cover the

dx.doi.org/10.1021/ic200011m |*Inorg. Chem.* XXXX, XXX, 000–000

Scheme 1. Synthesis of Precursors P1−P9 and Ligands L1−L7[a]

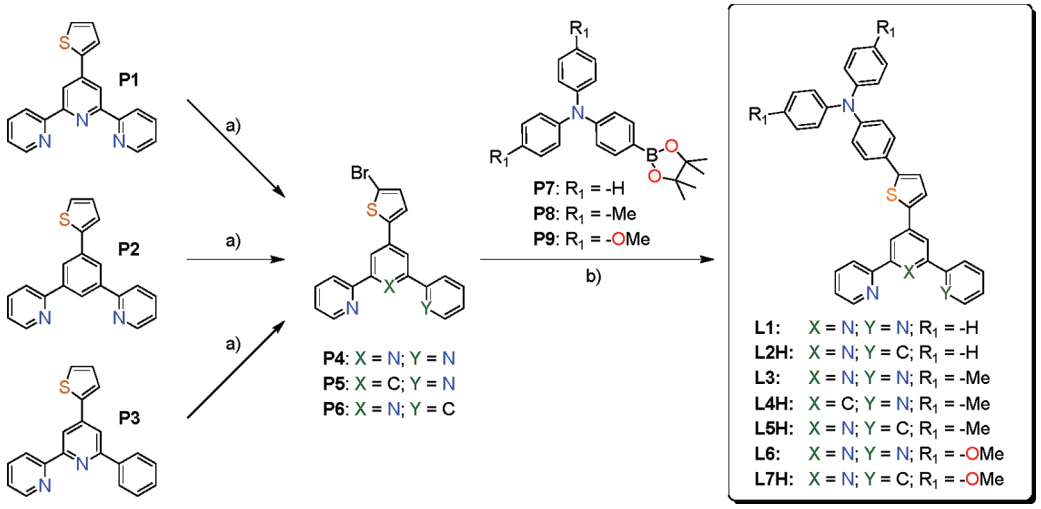

[a] Reaction conditions: (a) 1 equiv of NBS, THF/AcOH (2:1), RT, 8 h; (b) $Pd(PPh_3)_4$, K_2CO_3, THF:H_2O (9:1), 65 °C, 14 h.

devices. The measurement settling time between the application of a voltage and the measurement of the current for the I−V characterization of DSSCs was fixed to 40 ms. The measurement of incident photon-to-current conversion efficiency (IPCE) was plotted as a function of excitation wavelength by using the incident light from a 300 W xenon lamp (ILC Technology, U.S.A.), which was focused through a Gemini-180 double monochromator (Jobin Yvon Ltd.).

RESULTS AND DISCUSSION

The so-called "black dye", $[Ru(Htctpy)(NCS)_3](NBu_4)_3$ (Htctpy = doubly deprotonated form of H_3tctpy), remains one of the highest performance dyes in the DSSC,[81] yet the balance of Ru-based champion dyes in the literature contain bidentate ligands.[19] While dicationic polypyridyl Ru(II) complexes do not typically offer satisfactory performance in the DSSC, cyclometalating ligands provide the opportunity for effective sensitization because of the lower local symmetry about the metal and the opportunity for injection from a higher-energy state.[55] In this vein, we report herein a series of "black dye" analogues where the three NCS^- ligands are replaced by a tridentate chelating ligand equipped with a TPA-based chromophore that has the potential both to harvest more light and to enhance charge separation (Chart 1).

The ensuing discussion will offer an overview of the syntheses and structural characterization of the title complexes **1**−**15**. An analysis of the spectroscopic and redox behavior of these complexes will then be presented to delineate the effects of cyclometalation. It will then be demonstrated that the placement of the organometallic bond and substitution at the R_1 position offer synthetic handles for moving the position of the HOMO about the molecule (i.e., localized to the TPA unit or the metal chelate) in a controlled fashion to enable the convergence on high performance *bis*tridentate DSSC sensitizers. Note that substituents placed at R_2 were varied to aid the characterization of the complexes (e.g., $R_2 = -CO_2Me$ engenders greater solubility than the corresponding acid), but only the complexes where $R_2 = -CO_2H$ enable effective binding to TiO_2 for the DSSC.

Synthesis and Structural Characterization. A modular synthetic approach was developed to furnish a library of TPA-functionalized tridentate ligands where the position of the organometallic bond and electron-donating character of the TPA can be easily modulated (Scheme 1). The syntheses of each of these donor ligands were achieved in reasonably high yields and scales. Using the thiophene-functionalized *pro*-ligands **P1**−**P3** as a starting point, electrophilic bromination reactions mediated by NBS afford the brominated chelating portion of the donor ligands **P4**−**P6**, which are poised for carbon−carbon bond formation with triarylamine-based Suzuki reagents to furnish **L1**−**L7H**.

The construction of the cyclometalated complexes was generally more successful when the cyclometalation step followed the installation of the tpy-based fragment (Scheme 2). Consequently, the respective $Ru(N^\wedge N^\wedge N)Cl_3$ synthons were used to synthesize the cyclometalated complexes **2**−**4**, **6**−**11**, **13**−**15**. There are, however, notable byproducts that arise in varying amounts depending on the specific reaction conditions. One of these byproducts is the homoleptic complex, $[Ru(\mathbf{L6})_2]^{2+}$ (**16**), which is typically formed with yields of 20−30%; a description of the isolation of **16** during the synthesis targeting **13** is provided as a representative sample in the Experimental Section.

Complexes **4**, **9**, **11**, and **15** were each derivatized from **3**, **8**, **10**, and **14**, respectively, and therefore do not follow the protocols described in Scheme 2. Compounds **4**, **9**, **11**, and **15** were prepared by hydrolyzing the ester precursors using triethylamine in aqueous DMF. Metal complexes were readily purified using column chromatography and isolated in reasonable quantities.

The structural identities of all ligands and complexes were confirmed by a combination of NMR spectroscopy, mass spectrometry, and/or elemental analysis. The identity of each of the complexes can be unambiguously verified by $^1H/^{13}C$ NMR (1D and 2D) techniques owing to the sufficient separation of the aromatic signals and asymmetry of the complexes. A collection of representative ^1H NMR spectra for −Me substituted TPA derivatives (e.g., **5**, **6**, and **7**) are provided in Figure 2 to illustrate the effect of the installation and position of a Ru−C bond on the chemical shift values.

The relative electron-donating character of substituents positioned about the TPA ligand is evidenced by the progressively upfield ^1H signals for the TPA groups of **1** ($R_1 = -H$), **5** ($R_1 = -Me$), and **12**

dx.doi.org/10.1021/ic200011m |*Inorg. Chem.* XXXX, XXX, 000–000

Scheme 2. Assembly of Complexes 1−3, 5−8, 10, and 12−14[a]

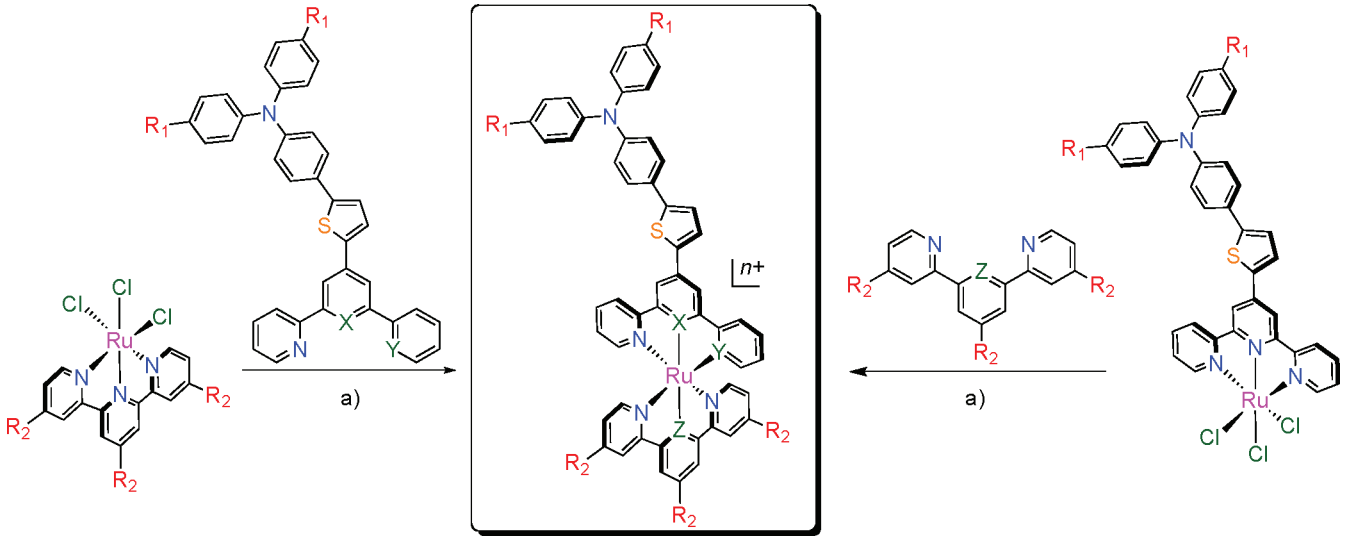

[a] Reaction conditions: (a) MeOH/H_2O/THF (5:1:1 *v*/*v*/*v*), *N*-ethylmorpholine, 65 °C, N_2, 14 h. R_1 = −H, −Me, −OMe; R_2 = −H, $-CO_2Me$, $-CO_2H$.

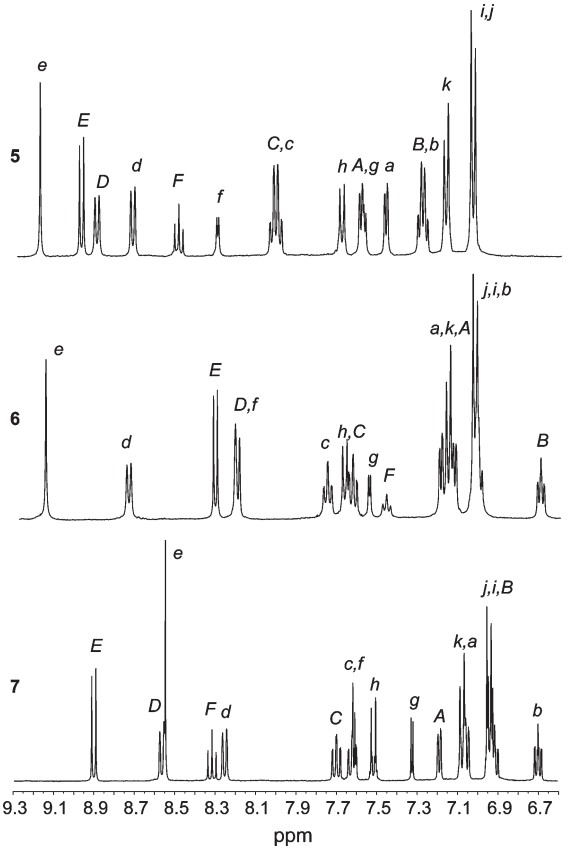

Figure 2. ^{1}H NMR spectra for d_4-MeOD solutions of **5**−**7** at ambient temperatures. Signals are assigned according to the labeling scheme provided in Figure 1.

(R_1 = −OMe). Following this same trend, the thiophene proton, H_g, is also shifted modestly upfield (e.g., H_g = 7.61, 7.55, 7.49 ppm for **1**, **5**, and **12**, respectively). The ^{1}H NMR signals corresponding to the protons of tpy bearing the thiophene-TPA unit were not affected by substitution at the TPA. Electron density of the TPA fragments are not affected by changing Z from N to C, as evidenced by the static position of H_h for **5** and **6**. The position of the H_e signal is sensitive to the position of the organometallic bond (i.e., 9.16, 9.13, and 8.53 ppm for **5**−**7**, respectively). In the case of **7**, where the central ring of the cyclometalating ligand participates in σ-bonding with the metal, the thiophene H_g and TPA H_h signals are also shifted upfield (H_g = 7.55 ppm and H_h = 7.67 ppm for **5**; H_g = 7.30 ppm and H_h = 7.50 ppm for **7**). The relative shifts of the thiophene and TPA proton signals are consistent with the anionic ligand in **7** donating electron density to both the Ru and TPA fragments (this statement is supported by electrochemical measurements; vide infra). When the anionic ring is on the tridentate ligand distal to the TPA-substituted ligand, the signals are shifted upfield (H_E = 8.29 for **6**) relative to the polypyridyl complex **5** (H_E = 8.95).

Solubility issues preclude the collection of ^{1}H NMR spectra for **8** and **14** in the same solvent, thereby making a direct comparison of the effect of the position of the Ru−C bond from the central ring to the adjacent ring difficult. There are, however, some distinctive NMR signals, including an upfield shift of the proton *ortho* to the organometallic bond (H_q = 5.37 ppm) for **14** − a feature that is indicative of cyclometalation. The spectra for **14** and **15** show the effect of the electron-withdrawing methylester and carboxylic acid groups; specifically, an upfield shift of H_E upon conversion of the methylester to the carboxylic acid group reflecting the greater electron-withdrawing character of the former.

Electrochemical and Photophysical Behavior. Cyclic voltammetry along with electronic absorption and emission data were used to delineate the role of the organometallic bond and terminal substituents. A full listing of relevant redox and spectroscopic data is collected in Table 1 (title and benchmark compounds) and Supporting Information, Table S1 (ligands). Electrochemical data for **4**, **9**, **11**, and **15** is not included because of solubility issues. Note that the electrochemistry, UV−vis and emission data were recorded in DCM, MeOH, and MeCN, respectively. This inconsistency is, among other reasons,[91] a

dx.doi.org/10.1021/ic200011m |*Inorg. Chem.* XXXX, XXX, 000–000

Table 1. Summary of Spectroscopic and Electrochemical Properties for Polypyridyl and Cyclometalated Complexes

	UV−vis absorbance data (nm)[a]	emission data		$E_{1/2}$ (V vs NHE)[d]	
compound	λ_{max} ($\varepsilon \times 10^3$ M^{-1} cm^{-1})	λ_{em} (nm)[b]	τ (ns); ϕ[c]	Ru(III)/Ru(II)	$TPA^{\bullet+}/TPA^0$
1	505 (35.4), 430[sh], 329[sh], 308 (57.0)	720 (510)	410 (0.98)[e]	[e]	1.22
		549 (425)	3.4 (1.10)[e]		
2	565 (25.0), 516 (24.9), 420 (45.7), 312[sh]	540 (420)	3.3 (1.08)[e]	0.87	1.23
3	681[sh] (3.5), 584[sh], 526 (26.7), 431 (39.4), 330 (42.4)	549 (429)	3.2 (1.02); 0.27	1.17	1.22
5	511 (33.3), 443[sh], 354[sh], 308[sh]	740 (510)	450 (1.11)[e]	[e]	1.14
		610 (450)	3.9 (1.05)[e]		
6	561 (21.8), 518 (21.6), 423 (37.7), 313[sh]	568 (426)	3.8 (1.07)[e]	0.88	1.15
7	536 (11.8), 505 (12.6), 391 (40.0), 314 (36.6)	502 (392)	3.2 (1.14)[e]	0.79	0.95
8	580 (13.9), 501 (18.4), 393 (47.5), 343 (42.3)	518 (396)	[e]	0.96[f]	0.96[f]
10	681[sh] (3.5), 584[sh], 526 (28.4), 435 (39.3), 330 (42.5)	561 (433)	3.6 (1.00); 0.24	1.17	1.11
12	516 (32.7), 451[sh], 352 (22.4), 308 (52.8)	730 (514)	[e]	[e]	1.00
13	566 (24.6), 517 (23.6), 426 (39.7), 314[sh]	[e]	[e]	0.88	1.01
14	681[sh] (2.9), 574[sh], 527 (29.6), 437 (37.5), 331 (41.0)	[e]	[e]	1.17	0.99
16	541 (63.7), 448 (23.6), 357 (44.7), 304[sh]	720 (541)	11.8 (0.99)[e]	[e]	1.00
17	475 (15.5), 308 (51.0)	619 (449)	[e]	1.52[g]	[e]

[a] Data collected in MeOH; ε values indicated in parentheses with units of $\times 10^3$ M^{-1} cm^{-1}. [b] Data collected in MeCN; λ_{ex} values indicated in parentheses with units of nm. [c] χ^2 indicated in parentheses; absolute quantum yield measured with an integrating sphere. [d] Data collected using 0.1 M NBu_4BF_4 CH_2Cl_2 solutions at 100 mV/s and referenced to a $[Fc]/[Fc]^+$ or $[OFc]/[OFc]^+$ internal standard followed by conversion to NHE; $[Fc]/[Fc^+]$ = +765 mV vs NHE in CH_2Cl_2; $[OFc]/[OFc]^+$ = +290 mV vs NHE in CH_2Cl_2. [e] Not observed. [f] Peaks resolved by 40 mV in differential pulse voltammetry (DPV) experiments recorded in MeCN. [g] Measured in MeCN with NBu_4BF_4. [sh] Shoulder.

consequence of the solvent medium affecting data resolution in certain cases. Data for **1**, **3**, and **8** recorded solely in MeCN (Supporting Information, Table S2) indicates that the solvent has a negligible effect on the optical properties, but affects the relative positions of the oxidation potentials (e.g., shifted by ca. −100 and −70 mV for the Ru(III)/Ru(II) and $TPA^{\bullet+}/TPA^0$ redox couples, respectively, in MeCN relative to CH_2Cl_2; Supporting Information, Figure S1). Differential pulse voltammetry (DPV) was employed to help resolve closely positioned oxidation waves. The absorption data for selected complexes were modeled by TD-DFT (Supporting Information).[92] The outcome of these results served as a guide for making reasonable assignments of the principal low-energy transitions for all complexes, an analysis made possible by the molecular asymmetry of the structures and the pseudo C_{2v} symmetry about the metal center. Taking these features into account along with the systematic variation within the series of the compounds, we are able to provide a complete assessment of the optical and electrochemical data below.

Role of the TPA Substituent. Analysis of each of the free TPA-substituted ligands reveals relatively broad intense absorption bands centered over the 381−415 nm range (Supporting Information, Figure S2) arising from a series of intramolecular $\pi \rightarrow \pi^*$ transitions emanating from the TPA fragment. (These same transitions are classified herein as ILCT transitions when the ligand is bound to the Ru metal center.) Polypyridyl complexes **1**, **5**, and **12** each display a prominent absorbance band centered within the 400−600 nm range due to MLCT and TPA-based ILCT transitions of comparable energies (Supporting Information, Figure S3).[59] Despite the electron-rich character of the TPA fragment, a computational analysis indicates that the extended conjugation of the thiophene bridge results in a slightly lower π^* orbital of the adjacent tpy chelate relative to the distal tpy ligand for **5** (Supporting Information, Figure S4). However, the presence of electron-withdrawing groups at R_2 (e.g., $-CO_2Me$, $-CO_2H$) leads to the LUMO being localized to the tpy chelate distal to the TPA-substituted ligand (denoted π^*_d).

The voltammograms for all of the polypyridyl complexes (e.g., **1**, **5**, **12**, and **16**) show a single quasi-reversible one-electron redox process ($E_{1/2}$ = +0.99−1.22 V) corresponding to the oxidation of the TPA unit (i.e., $TPA^{\bullet+}/TPA^0$). A sweep to more oxidizing potentials renders an irreversible oxidation wave that compromises the direct measure of the Ru(III)/Ru(II) redox couple, but is presumably comparable to the oxidation potential of +1.5 V for $[Ru(tpy)_2]^{2+}$ (**17**).[55] The reductive scans produce an irreversible signal with an onset of about −0.8 V. This reductive behavior was observed for all of the metal complexes and TPA-substituted ligands in this study thereby disabling an estimation of the thermodynamic position of the LUMO by electrochemical methods.

Effects of Cyclometalation. An anodic sweep of each of the cyclometalated complexes in Chart 1 produces two consecutive single-electron processes. In the case of **2**, these redox waves are assigned as the successive oxidation of the metal and TPA units (Figure 3a). This situation, which is different from that of **1** in that it indicates a metal-based HOMO, is consistent with the anionic cyclometalating ligand lowering the formal oxidation potential of octahedral Ru(II) center.[37,54−56] Indeed, the dpb^- ligand of **2** lowers the Ru(III)/Ru(II) redox couple by about 600 mV versus NHE relative to **17**. This trend holds for all of the cyclometalated complexes; however, the magnitude of the cathodic shift depends on the position of the Ru−C bond and substituents around the periphery of the distal ligand (vide infra). Note that the $TPA^{\bullet+}/TPA^0$ redox wave remains static for **1** and **2** (∼+1.23 V vs NHE), thus indicating that electron density at the metal site has little effect on the TPA unit when Z = C (Chart 1).

The UV−vis spectra in Figure 3a illustrate how replacing one Ru−N bond with a Ru−C bond significantly affects the optical properties. While the polypyridyl complexes are characterized by an intense absorption band (e.g., 505 nm for **1**), anionic

dx.doi.org/10.1021/ic200011m |*Inorg. Chem.* XXXX, XXX, 000–000

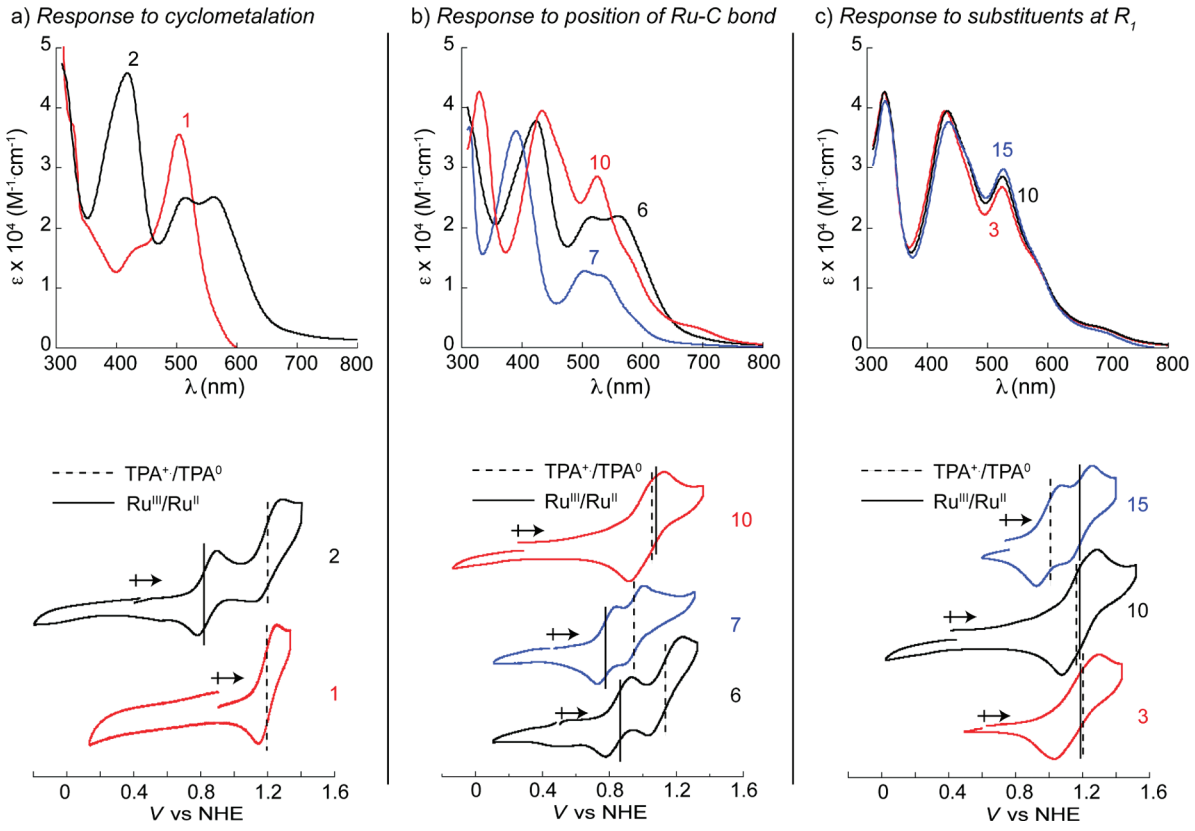

Figure 3. UV−vis spectra in MeOH and cyclic voltammograms in CH_2Cl_2 for select compounds highlighting the effect of the optical and electrochemical properties upon (a) the introduction of an organometallic bond; (b) varying the position of the organometallic bond; (c) increasing the electron-donating character of R_1. Vertical lines represent Ru(III)/Ru(II) (solid) and $TPA^{\bullet+}/TPA^0$ (dashed) $E_{1/2}$ values.

cyclometalating ligands lower the degeneracy of the frontier orbitals thus separating the ILCT and MLCT transitions to render a broader absorption envelope. The electron density imparted on the Ru center by the anionic ligand, for example, bathochromically shifts the MLCT transitions because the tpy-based π^* orbitals are raised to higher energies to a lesser extent than the metal-based orbitals.[54,55] The nature of the orbitals participating in the ILCT and MLCT transitions is provided as Supporting Information for select complexes (e.g., **5**−**7**; Supporting Information, Figures S4−S6). It is found that the ILCT transitions arise from the TPA unit to the π^* system of the proximate chelate (π^*_p), and the MLCT transitions emanate from three filled metal-based orbitals to the π^* systems of the chelate either distal (π^*_d) or proximate (π^*_p) to the TPA unit (i.e., $d_{yz} \rightarrow \pi^*_p$, $d_{xz} \rightarrow \pi^*_d$, $d_{xy} \rightarrow \pi^*_p$, $d_{xy} \rightarrow \pi^*_d$; the relative positions of said orbitals are provided in Figure 4). [We caution that there is significant orbital mixing within the multielectron wave functions; thus, the orbital notation used herein (e.g., d_{xy}, π_{TPA}, etc.) merely reflects predominant orbital character to simplify the discussion; see Supporting Information, Figure S4 caption for further details.] Taking the experimental and computational data into collective account, the introduction of the organometallic bond leads to the following key perturbations: (i) the metal orbital that interacts with the anionic ring is pushed up in energy by 770−900 mV (the other filled metal orbitals are destabilized to a slightly lesser extent); (ii) the π^* orbitals of the cyclometalating tridentate ligands move up in energy by ∼700 mV; and (iii) the π^* orbitals of the neutral ligands are shifted to higher energies by ∼300 mV.[93]

Position of the Organometallic Bond. The differences in the optical spectra of **6**, **7**, and **10**, a series where the C is positioned at Z, X, and Y, respectively (Chart 1), can be attributed largely to the variability in the energies of the ILCT transitions (Figure 3). In the case of **6**, an ILCT transition promotes an electron to the π_p^* orbital of a neutral tpy chelate, while the same transition for **7** involves a π_p^* orbital localized to the anionic dpb^- ligand. Because the π_p^* orbital is higher in energy for **7**, the ILCT transitions are pushed below 400 nm thus suppressing the intensity of the absorption manifold in the visible region.

Visible light absorption is enhanced when the organometallic bond involves a flanking ring of the chelate proximate to the TPA unit (e.g., **10**). In this situation, the Ru $\rightarrow \pi_p^*$ MLCT transitions occur at $\lambda_{max} > 350$ nm because the central ring of $pbpy^-$, which is in direct conjugation with the TPA unit, is neutral. (In comparing **6** and **7** to **10**, note that the $-CO_2Me$ groups induce a slight red-shift in the optical transitions.) The symmetry of **10** produces spectral changes that correspond to the expected reordering of the energy levels: the d_{xy} orbital is the highest-energy filled metal orbital; the π^*_d orbitals reside at lower energies than those of **7** because of the electron-withdrawing $-CO_2Me$ groups; and the π_{TPA} is lower in energy relative to **7** because of the lack of direct conjugation between the TPA fragment and anionic ring. A summary of the relative positions of the energy levels is provided in Figure 4.

Altering the position of the organometallic bond about the Ru metal also induces significant changes in the electrochemical properties (Figure 3b). The CV for **6** consists of two quasi-reversible oxidation waves at about +0.88 and +1.15 V vs NHE

dx.doi.org/10.1021/ic200011m |*Inorg. Chem.* XXXX, XXX, 000–000

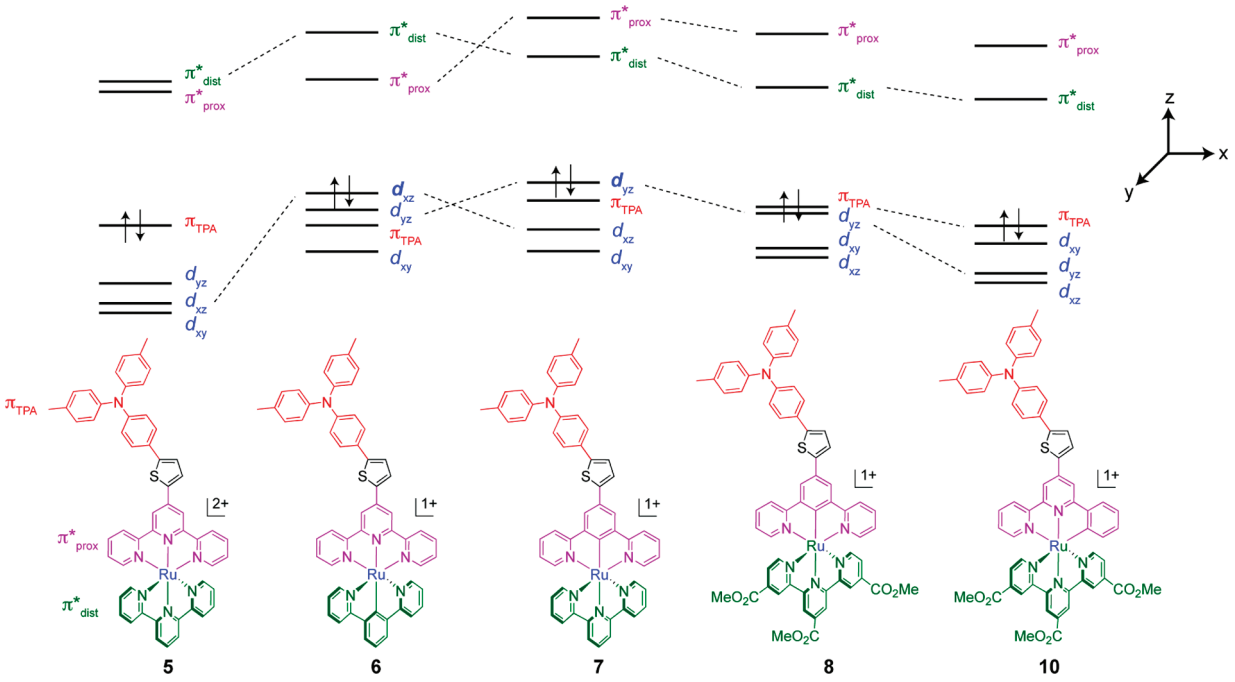

Figure 4. Qualitative energy level diagram for **5**−**8** and **10** illustrating that the HOMO can be localized to the TPA unit (e.g., **5**, **8**, and **10**) or the metal chelate (e.g., **6**, **7**) depending on the position of the Ru−C bond. (Compound **8** is included to show how the $-CO_2Me$ groups affect the energy levels of **10**; the dashed lines are provided as a guide for the reader; electrons indicate HOMO.). $\pi^*_p = \pi^*$ of the tridentate chelate proximate to the TPA; $\pi^*_d = \pi^*$ of the tridentate chelate distal to the TPA.

assigned as Ru(III)/Ru(II) and $TPA^{\bullet+}/TPA^{0}$ redox couples, respectively. Moving the organometallic bond to the opposite side of the metal (e.g., **7**) leads to a ∼100 mV cathodic shift of both oxidation potentials. A notable feature for **7**, where the anionic ring is in direct conjugation with the TPA fragment, is that the Ru(III)/Ru(II) redox couple is affected by substituents at R_1. The central anionic ring therefore appears to mediate electronic communication between the TPA fragment and the Ru center; the NMR data is aligned with this claim.

In the case of **10**, the metal-based oxidation potential is shifted to substantially more positive potentials such that the first oxidation wave for the complex involves the TPA unit (Figure 3). This observation, which indicates that the HOMO is localized to the TPA unit rather than the metal (Figure 4), is an unprecedented finding for cyclometalated sensitizers. This data also highlights that the proximity of the anionic ring to the electron-rich TPA unit leads to a significantly different order in the frontier molecular orbitals for **6**, **7**, and **10**.

Substituent Effects at the R_1 Position of the TPA Unit. The above experiments reveal independent control of the oxidation potentials of the TPA and metal units when the Ru−C bond is not proximal to the TPA-bearing units (e.g., **10**). This result inspired us to fine-tune the frontier molecular orbitals by altering the R_1 groups. We found that varying the substituents at the R_1 position has a very minor effect on the optical properties when the balance of the structure is held at parity. The UV−vis absorption spectra for **3**, **10**, and **15**, for example, display only a slight bathochromic shift for R_1 = −H, −Me, and −OMe, respectively (Figure 3c). This same trend holds for the polypyridyl complexes **1**, **5**, and **12** (Supporting Information, Figure S3).

The redox behavior of the TPA unit, on the other hand, is significantly affected by substitution at the R_1 position. As expected, the TPA unit is more easily oxidized with electron-rich substituents; for example, the TPA oxidation potentials are lowered from +1.22 to +0.99 V when R_1 is changed from −H to −OMe for the cyclometalated complexes where Y = C and R_2 = $-CO_2Me$ (e.g., **3**, **14**). Cathodic shifts of similar magnitudes are observed for the noncyclometalated analogues **1** and **12**. Substituents at R_1 do not, however, affect the Ru(III)/Ru(II) oxidation potential when the Ru−C bond is *not* in direct conjugation with the TPA unit (e.g., the Ru(III)/Ru(II) couple appears at ∼+0.89 vs NHE for **2**, **6**, and **13**). In cases where X = C (Chart 1), the Ru(III)/Ru(II) and $TPA^{\bullet+}/TPA^{0}$ redox couples converge when R_2 is an electron-rich substituent.

These results illustrate that independent control of the oxidation energy levels of the two redox-active centers enables the manipulation of the position of the HOMO about the complex. When R_1 = −H and Y = C (**3**), for example, the first oxidation process is predominantly metal-based. The oxidation of **14** (R_1 = −OMe; Y = C), however, involves the removal of an electron from the TPA unit prior to the oxidation of the metal. This finding is important for our goal of sensitizing TiO_2 because the latter scenario provides an energetic landscape that leaves open the opportunity for suppressing charge recombination via an electronic cascade mechanism; that is, the excited-energy levels are appropriately positioned for funneling a photoexcited electron into TiO_2 (the LUMO is localized to **L11**), and the ground-state energy levels are positioned to accommodate hole-transfer from the metal to the TPA unit following a light-induced MLCT event (Figure 5). We therefore set out to explore the viability of these assemblies as sensitizers in the DSSC.

Solar Cell Performance. With a detailed understanding of the electrochemical and photophysical properties in hand, we examined the performance of relevant complexes in the DSSC,

dx.doi.org/10.1021/ic200011m |*Inorg. Chem.* XXXX, XXX, 000–000

Table 2. Solar Cell Performance Parameters Obtained Under Simulated AM 1.5 Illumination for Select Dyes

compound	electrolyte	J_{sc} (mA/cm^2)	V_{oc} (mV)	fill factor	η (%)
4	Z960	10.81	677	0.74	5.41
	Z1137	14.95	672	0.71	7.13
9	Z960	8.49	542	0.73	3.36
	Z1137	8.26	608	0.77	3.90
11	Z960	10.03	594	0.74	4.41
	Z1137	13.00	653	0.75	6.33
15	Z960	11.61	686	0.73	5.81
	Z1137	16.74	682	0.71	8.02
N3	Z960	16.76	752	0.74	9.32
	Z1137	16.48	713	0.74	8.65

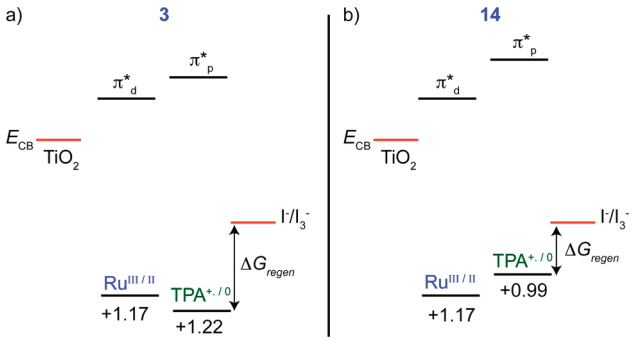

Figure 5. Thermodynamic positions of the frontier molecular orbitals of (a) **3** and (b) **14** relative to the conduction band (E_{CB}) of TiO_2 and the I^-/I_3^- redox couple. The relative positions of the energy levels for **14** are conducive to shuttling electrons toward TiO_2 and holes toward the terminal TPA unit to interact with the redox mediator following excitation. The energy levels for **3** should not, in principle, accommodate this same effect. Note that ΔG_{regen} (the driving force for the reaction between I^- and the oxidized TPA unit) is greater for **3** than **14**, yet the performance of the acid analogues (i.e., **4** and **15**) in the DSSC is greater for **14**.

namely, those complexes bearing $-CO_2H$ anchoring groups: **4**, **9**, **11**, and **15**. The performance of related cyclometalated sensitizers and the sensitizers and **N3** are included as benchmark compounds. Parameters extracted from the measured current−voltage ($I-V$) traces under standard AM 1.5 sunlight [e.g., the open circuit voltage (V_{oc}); short circuit photocurrent density (J_{sc}); fill factor; η] are detailed in Table 2; the reported values are average measurements of three different cells with margins of error of ±0.2%. The sensitizers were screened employing two liquid electrolytes denoted as Z960 (i.e., 1.0 M 1,3-dimethylimidazolium iodide (DMII), 30 mM I_2, 0.5 M *tert*-butylpyridine, 0.05 M LiI and 0.1 M guanidinium thiocyanate (GNCS) in the mixed solvent system of acetonitrile and valeronitrile [*v*/*v*, 85/15]) and Z1137 (i.e., 1.0 M 1,3- dimethylimidazolium iodide (DMII), 60 mM I_2, 0.5 M *tert*-butylpyridine, 0.05 M NaI and 0.1 M GuNCS in a mixed solvent system of acetonitrile and valeronitrile (*v*/*v*, 85/15). Note that the UV−vis and redox behavior for the sensitizers could not be ascertained because of solubility reasons, but useful comparisons are provided by the corresponding methylester derivatives (e.g., **8** and **9**, **10**, and **11**, etc.)

The relative photovoltaic performance of **9** and **11** offers insight into the importance of the *position* of the organometallic

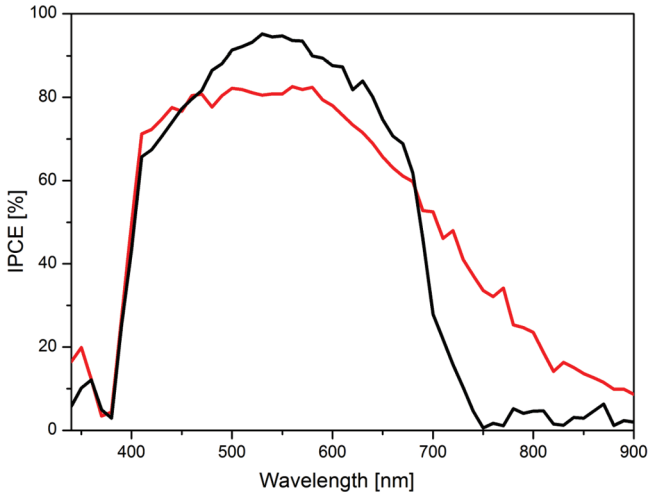

Figure 6. Photocurrent action spectrum obtained for **15** (red line) attached to nanocrystalline TiO_2 films using the Z1137 electrolyte. The photocurrent action spectrum for **N3** (black line) measured under similar conditions is also included for comparison.

bond: η is almost 40% greater for **11** when the cyclometalating ligand is positioned on the flanking ring rather than the central ring. This feature is primarily due to the inferior light-harvesting capacity of **9** in the visible region that is manifest in the anionic ring increasing the energies of the ILCT transitions. Note that in the case of **11**, the anionic phenyl ring and the TPA-substituted pyridyl ring both reside *trans* to pyridyl rings bearing acid linkers. Positioning the anionic ring within the tridentate chelate proximate to the TPA unit also enables *three* acid groups to be positioned on the distal tpy ligand for optimal binding and interaction with the TiO_2 surface.[94] Consequently, the molecular motif where the flanking ring is anionic (e.g., Y = C) is optimal for sensitizing TiO_2 among the series in Chart 1.

Data for **4**, **11**, and **15**, a series with similar optical profiles where only the substituents about the TPA unit are varied, lends some insight into the importance of the relative thermodynamic positions of the TPA and metal chelate. Because the HOMO is localized to the TPA unit for **11** and **15** rather than the Ru chelate,[95] the relative energy levels have the potential to facilitate rapid hole transfer toward the TPA unit to interact with the electrolyte (illustrated for $-CO_2Me$ analogues in Figure 5).[60,62,71] This same process should, in principle, be suppressed for **4** because oxidation of the TPA by the photo-oxidized metal unit is endergonic. The higher value for **15** relative to **4** lends indirect support to such an effect (note that both complexes are characterized by similar optical profiles). While the data for **11** does not adhere to a trend that supports our proposal, we note that Me-substituted TPA donor units in organic dyes have a tendency to generate lower performance in the DSSC than TPAs bearing other substituents.[96] Transient spectroscopic studies are underway to verify our hypothesis of an electronic cascade effect following light absorption, and to unravel other factors that may affect performance (e.g., chemical interaction with the electrolyte[65,97,98]).

The incident photon-to-electricity conversion efficiency (IPCE) spectrum for **15** shows a maximum of about 83% and appreciable response out to 650 nm (Figure 6). This result confirms that the majority of the light harvested by both the metal chelate and the TPA unit is being converted into useful electrical energy and

dx.doi.org/10.1021/ic200011m |*Inorg. Chem.* XXXX, XXX, 000–000

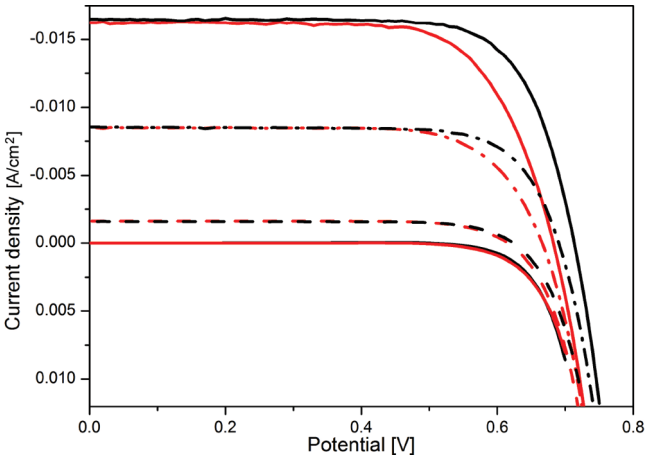

Figure 7. Comparison of $I-V$ characteristics for **15** (red line) and **N3** (black line) at 1 sun (solid lines), 0.5 sun (dash-dotted lines), and 0.1 sun (dash lines) using the Z1137 electrolyte. Solid lines at 0 A/cm^2 are dark current measurements.

corroborates the LUMO being localized to **L11**. It is also noteworthy that **15** shows an IPCE of 10% at 900 nm, whereas the IPCE for **N3** is negligible at wavelengths as short as 750 nm, thereby demonstrating the panchromatic response for this class of cyclometalated sensitizers.

Figure 7 shows a comparison of the device characteristics for **15** and **N3** at variable light intensities. The data reveals a high photocurrent density (J_{sc}) for both sensitizers; however, the open circuit voltage (V_{oc}) for **15** is 30 mV lower than that of **N3**. The relatively higher V_{oc} for **N3** is tentatively ascribed to a combination of the higher directionality and dipole influence of the **N3** sensitizer, but the interaction of the TPA unit with the electrolyte may also adversely affect the V_{oc}.[98] Indeed, the electrolyte composition is found to have a significant influence on the current−voltage characteristics and power conversion efficiencies of the cyclometalated dyes in Table 2 based on Z960 and Z1137 electrolytes. Further studies are underway to study the behavior of these dyes in various dye uptake experiments with electrolytes and in solid-state DSSC architectures.

SUMMARY

Previous studies have shown that the NCS$^-$ ligands of **N3** can be replaced with bidentate cyclometalating ligands without compromising DSSC performance to a significant extent.[28] Replacing the NCS$^-$ ligands of the "Black Dye" (i.e., [Ru(Htctpy)(NCS)$_3$][(NBu$_4$)$_3$]) with anionic tridentate chelating ligands, however, is only recently gaining attention.[27,31,32,56] In this vein, this article systematically unravels factors critical to improving the performance of tridentate cyclometalated Ru dyes in the DSSC. To gain a fundamental understanding of the photophysical properties of this particular class of dyestuff, we developed an extensive series of asymmetric cyclometalated Ru(II) complexes bearing a TPA light-harvesting unit bridged by a thiophene to further enhance light absorption.[59] This platform is accessible by a modular synthetic approach involving well-established coupling and condensation techniques, and a full physicochemical assessment is made possible by the dissymmetry of the molecular topology, the local symmetry about the metal center, and the systematic installation of EWGs and EDGs about the periphery of the molecule.

While broad absorption spectra are generated in Ru(II) complexes containing an organometallic bond because of the electronic dissymmetry about the octahedral Ru(II) center, the intensity of the spectra in the visible region is enhanced when the organometallic bond is *orthogonal* to the principal axis (e.g., Y = C). Cases where Z = C are not ideal for light-harvesting because the LUMO is localized to the tridentate chelate remotely positioned from the surface (i.e., π^*_p). When X = C, the ILCT transitions are shifted toward the UV region thus shunting the optical response in the visible region. We therefore conclude that the placement of the anionic ring on the flanking position of the tridentate ligand proximate to the TPA unit maximizes light harvesting in the visible region, maintains sufficient vectoral electron transfer toward the semiconductor surface, and ensures that the LUMO is situated on the anchoring ligand to enable facile charge injection into the TiO_2.

This study also highlights the ability to independently manipulate the thermodynamic energy levels of the redox-active TPA and metal units. Because the TPA and metal-based oxidation potentials can range from +0.95−1.22 V and +0.88−1.52 V, respectively, the HOMO can be positioned on either the metal or the TPA fragment through the judicious choice of R_1 and proper placement of the organometallic bond. This feature is critical for meeting our overarching goal of inducing an electronic cascade effect,[71] which is inherently dependent on the position of the HOMO. For example, electron−rich substituents installed on the TPA group and Y = C (e.g., **15**) yield an arrangement of HOMO (TPA-based) and HOMO-1 (metal-based) levels that favors the movement of photoinduced holes toward the TPA unit (e.g., Figure 5) following a MLCT event thus achieving a high performance in the DSSC. Further studies are underway to directly probe this effect.

Our systematic approach to dye design revealed that the absorption profiles and the photoaction spectra of these systems can be extended beyond 750 nm. The culmination of this work shows that the proper design of hybridized organometallic/organic dyes devoid of NCS$^-$ ligands are capable of generating high η values in the DSSC (i.e., >8%). This value is significantly higher than previously reported *bis*tridentate Ru sensitizers,[19,27] with the exception of a study that emerged while this article was under review.[32] Studies are underway to examine the performance of these dyes in solid-state DSSC architectures and to time-resolve the excitation and injection processes.

ASSOCIATED CONTENT

Supporting Information. Physicochemical data for **L1**−**L7H**, physicochemical data select complexes in MeCN, UV−vis absorption spectra, TD-DFT analysis of **5**−**7**. This material is available free of charge via the Internet at http://pubs.acs.org.

AUTHOR INFORMATION

Corresponding Author
*E-mail: cberling@ucalgary.ca.

ACKNOWLEDGMENT

This work was financially supported by the Canadian Natural Science and Engineering Research Council (NSERC), Canada Research Chairs, Canadian Foundation for Innovation (CFI),

Alberta Ingenuity, Canada School of Energy and Environment (CSEE). We are also grateful to NSERC (KCDR, BS) and Alberta Innovates (KCDR) for scholarships, Eduardo Schott for assistance with DFT studies, and to an anonymous reviewer of this paper for constructive comments. M.K.N. thanks the EU SPI-Cooperation, Collaborative Large-scale integrating project ORION FP7-NMP-LA-2009-229036, and World Class University (WCU) program funded by the Ministry of Education, Science and Technology (Grant R31-2008-000-10035-0).

REFERENCES

(1) Juris, A.; Balzani, V.; Barigelletti, F.; Campagna, S.; Belser, P.; Von Zelewsky, A. *Coord. Chem. Rev.* **1988**, *84*, 85–277.
(2) Campagna, S.; Puntoriero, F.; Nastasi, F.; Bergamini, G.; Balzani, V. *Top. Curr. Chem.* **2007**, *280*, 117–214.
(3) Concepcion, J. J.; Jurss, J. W.; Brennaman, M. K.; Hoertz, P. G.; Patrocinio, A. O. T.; Murakami Iha, N. Y.; Templeton, J. L.; Meyer, T. J. *Acc. Chem. Res.* **2009**, *42*, 1954–1965.
(4) Abrahamsson, M.; Jäger, M.; Kumar Rohan, J.; Österman, T.; Persson, P.; Becker, H.-C.; Johansson, O.; Hammarström, L. *J. Am. Chem. Soc.* **2008**, *130*, 15533–42.
(5) Wasylenko, D. J.; Henderson, M. A.; Ganesamoorthy, C.; Koivisto, B. D.; Osthoff, H. G.; Berlinguette, C. P. *J. Am. Chem. Soc.* **2010**, *132*, 16094–16106.
(6) Padilla-Tosta, M. E.; Lloris, J. M.; Martinez-Manez, R.; Pardo, T.; Soto, J.; Benito, A.; Marcos, M. D. *Inorg. Chem. Commun.* **2000**, *3*, 45–48.
(7) Barigelletti, F.; Flamigni, L.; Calogero, G.; Hammarström, L.; Sauvage, J.-P.; Collin, J.-P. *Chem. Commun.* **1998**, 2333–2334.
(8) Yang, X.-J.; Drepper, F.; Wu, B.; Sun, W.-H.; Haehnel, W.; Janiak, C. *Dalton Trans* **2005**, 256–267.
(9) Beer, P. D.; Cadman, J. *Coord. Chem. Rev.* **2000**, *205*, 131–155.
(10) Argazzi, R.; Murakami Iha, N. Y.; Zabri, H.; Odobel, F.; Bignozzi, C. A. *Coord. Chem. Rev.* **2004**, *248*, 1299–1316.
(11) Angell, S. E.; Zhang, Y.; Rogers, C. W.; Wolf, M. O.; Jones, W. E. *Inorg. Chem.* **2005**, *44*, 7377–7384.
(12) Cooke, M. W.; Hanan, G. S. *Chem. Soc. Rev.* **2007**, *36*, 1466–1476.
(13) O'Regan, B.; Grätzel, M. *Nature* **1991**, *353*, 737–740.
(14) Grätzel, M. *Nature* **2003**, *421*, 586–587.
(15) Grätzel, M. *Acc. Chem. Res.* **2009**, *42*, 1788–1798.
(16) Grätzel, M. *J. Photochem. Photobiol. A* **2004**, *164*, 3–14.
(17) Green, M. A.; Emery, K.; Hishikawa, Y.; Warta, W. *Prog. Photovoltaics* **2010**, *18*, 144–150.
(18) Chiba, Y.; Islam, A.; Watanabe, Y.; Komiya, R.; Koide, N.; Han, L. *Jpn. J. Appl. Phys.* **2006**, *45*, L638–L640.
(19) Hagfeldt, A.; Boschloo, G.; Sun, L.; Kloo, L.; Pettersson, H. *Chem. Rev.* **2010**, *110*, 6595–6663.
(20) Grätzel, M. *Inorg. Chem.* **2005**, *44*, 6841–6851.
(21) Ardo, S.; Meyer, G. J. *Chem. Soc. Rev.* **2009**, *38*, 115–164.
(22) Durrant, J. R.; Haque, S. A.; Palomares, E. *Coord. Chem. Rev.* **2004**, *248*, 1247–1257.
(23) Kuciauskas, D.; Monat, J. E.; Villahermosa, R.; Gray, H. B.; Lewis, N. S.; McCusker, J. K. *J. Phys. Chem. B* **2002**, *106*, 9347–9358.
(24) Robertson, N. *Angew. Chem., Int. Ed.* **2006**, *45*, 2338–2345.
(25) Hamann, T. W.; Jensen, R. A.; Martinson, A. B. F.; Van Ryswyk, H.; Hupp, J. T. *Energy Environ. Sci.* **2008**, *1*, 66–78.
(26) Wang, P.; Klein, C.; Humphry-Baker, R.; Zakeeruddin, S. M.; Grätzel, M. *J. Am. Chem. Soc.* **2005**, *127*, 808–809.
(27) Wadman, S. H.; Kroon, J. M.; Bakker, K.; Lutz, M.; Spek, A. L.; van Klink, G. P. M.; van Koten, G. *Chem. Commun.* **2007**, 1907–1909.
(28) Bessho, T.; Yoneda, E.; Yum, J.-H.; Guglielmi, M.; Tavernelli, I.; Imai, H.; Rothlisberger, U.; Nazeeruddin, M. K.; Grätzel, M. *J. Am. Chem. Soc.* **2009**, *131*, 5930–5934.
(29) Bessho, T.; Zakeeruddin, S.; Yeh, C. Y.; Diau, E. G.; Grätzel, M. *Angew. Chem., Int. Ed.* **2010**, *49*, 6646–6649.
(30) Zeng, W.; Cao, Y.; Bai, Y.; Wang, Y.; Shi, Y.; Zhang, M.; Wang, F.; Pan, C.; Wang, P. *Chem. Mater.* **2010**, *22*, 1915–1925.
(31) Wu, K.-L.; Hsu, H.-C.; Chen, K.; Chi, Y.; Chung, M.-W.; Liu, W.-H.; Chou, P.-T. *Chem. Commun.* **2010**, *46*, 5124–5126.
(32) Chou, C.-C.; Wu, K.-L.; Chi, Y.; Hu, W.-P.; Yu, S. J.; Lee, G.-H.; Lin, C.-L.; Chou, P.-T. *Angew. Chem., Int. Ed.* **2011**, *50*, 2054–2058.
(33) Constable, E. C.; Hannon, M. J. *Inorg. Chim. Acta* **1993**, *211*, 101–110.
(34) Constable, E. C.; Thompson, A.; Tocher, D. A.; Daniels, M. A. M. *New J. Chem.* **1992**, *16*, 855–867.
(35) Constable, E. C.; Housecroft, C. E. *Polyhedron* **1990**, *9*, 1939–1947.
(36) Constable, E. C.; Leese, T. A. *J. Organomet. Chem.* **1987**, *335*, 293–299.
(37) Constable, E. C.; Holmes, J. M. *J. Organomet. Chem.* **1986**, *301*, 203–208.
(38) Collin, J. P.; Beley, M.; Sauvage, J. P.; Barigelletti, F. *Inorg. Chim. Acta* **1991**, *186*, 91–93.
(39) Patoux, C.; Launay, J.-P.; Beley, M.; Chodorowski-Kimmes, S.; Collin, J.-P.; James, S.; Sauvage, J.-P. *J. Am. Chem. Soc.* **1998**, *120*, 3717–3725.
(40) Jäger, M.; Smeigh, A.; Lombeck, F.; Görls, H.; Collin, J.-P.; Sauvage, J.-P.; Hammarström, L.; Johansson, O. *Inorg. Chem.* **2010**, *49*, 374–376.
(41) Maestri, M.; Balzani, V.; Deuschel-Cornioley, C.; Von Zelewsky, A. *Adv. Photochem.* **1992**, *17*, 1–68.
(42) Djukic, J. P.; Sortais, J. B.; Barloy, L.; Pfeffer, M. *Eur. J. Inorg. Chem.* **2009**, 817–853.
(43) Chi, Y.; Chou, P.-T. *Chem. Soc. Rev.* **2010**, *39*, 638–655.
(44) Gandolfi, C.; Heckenroth, M.; Neels, A.; Laurenczy, G.; Albrecht, M. *Organometallics* **2009**, *28*, 5112–5121.
(45) Sasaki, I.; Vendier, L.; Sournia-Saquet, A.; Lacroix, P. G. *Eur. J. Inorg. Chem.* **2006**, 3294–3302.
(46) Chi, Y.; Chou, P.-T. *Chem. Soc. Rev.* **2007**, *36*, 1421–1431.
(47) Zhong, Y.-W.; Wu, S.-H.; Burkhardt, S. E.; Yao, C.-J.; Abruña, H. D. *Inorg. Chem.* **2011**, *50*, 517–524.
(48) Yao, C.-J.; Sui, L.-Z.; Xie, H.-Y.; Xiao, W.-J.; Zhong, Y.-W.; Yao, J. *Inorg. Chem.* **2010**, *49*, 8347–8350.
(49) Sun, Y.; El Ojaimi, M.; Hammitt, R.; Thummel, R. P.; Turro, C. *J. Phys. Chem. B* **2010**, *114*, 14664–14670.
(50) Jacko, A. C.; McKenzie, R. H.; Powell, B. J. *J. Mater. Chem.* **2010**, *20*, 10301–10307.
(51) Collin, J. P.; Kayhanian, R.; Sauvage, J. P.; Calogero, G.; Barigelletti, F.; DeCian, A.; Fischer, J. *Chem. Commun.* **1997**, 775–776.
(52) Alonso-Vante, N.; Nierengarten, J.-F.; Sauvage, J.-P. *J. Chem. Soc., Dalton Trans.* **1994**, 1649–1654.
(53) Beley, M.; Chodorowski, S.; Collin, J.-P.; Sauvage, J.-P.; Flamigni, L.; Barigelletti, F. *Inorg. Chem.* **1994**, *33*, 2543–2547.
(54) Wadman, S. H.; Lutz, M.; Tooke, D. M.; Spek, A. L.; Hartl, F.; Havenith, R. W. A.; van Klink, G. P. M.; van Koten, G. *Inorg. Chem.* **2009**, *48*, 1887–1900.
(55) Bomben, P. G.; Robson, K. C. D.; Sedach, P. A.; Berlinguette, C. P. *Inorg. Chem.* **2009**, *48*, 9631–9643.
(56) Koivisto, B. D.; Robson, K. C. D.; Berlinguette, C. P. *Inorg. Chem.* **2009**, *48*, 9644–9652.
(57) Bomben, P. G.; Koivisto, B. D.; Berlinguette, C. P. *Inorg. Chem.* **2010**, *49*, 4960–4971.
(58) Asghar, M. I.; Miettunen, K.; Halme, J.; Vahermaa, P.; Toivola, M.; Aitola, K.; Lund, P. *Energy Environ. Sci.* **2010**, *3*, 418–426.
(59) Robson, K. C. D.; Koivisto, B. D.; Gordon, T. J.; Baumgartner, T.; Berlinguette, C. P. *Inorg. Chem.* **2010**, *49*, 5335–5337.
(60) Bonhôte, P.; Moser, J.-E.; Humphry-Baker, R.; Vlachopoulos, N.; Zakeeruddin, S. M.; Walder, L.; Grätzel, M. *J. Am. Chem. Soc.* **1999**, *121*, 1324–1336.
(61) Snaith, H. J.; Karthikeyan, C. S.; Petrozza, A.; Teuscher, J.; Moser, J. E.; Nazeeruddin, M. K.; Thelakkat, M.; Grätzel, M. *J. Phys. Chem. C* **2008**, *112*, 7562–7566.
(62) Karthikeyan, C. S.; Wietasch, H.; Thelakkat, M. *Adv. Mater.* **2007**, *19*, 1091–1095.
(63) Balzani, V.; Juris, A.; Barigelletti, F.; Belser, P.; Von Zelewsky, A. *Sci. Pap. Inst. Phys. Chem. Res. (Jpn.)* **1984**, *78*, 78–85.

(64) Abrahamsson, M.; Jäger, M.; Österman, T.; Eriksson, L.; Persson, P.; Becker, H.-C.; Johansson, O.; Hammarström, L. *J. Am. Chem. Soc.* **2006**, *128*, 12616–12617.
(65) Hagberg, D. P.; Marinado, T.; Karlsson, K. M.; Nonomura, K.; Qin, P.; Boschloo, G.; Brinck, T.; Hagfeldt, A.; Sun, L. *J. Org. Chem.* **2007**, *72*, 9550–9556.
(66) Klumpp, T.; Linsenmann, M.; Larson, S. L.; Limoges, B. R.; Buerssner, D.; Krissinel, E. B.; Elliott, C. M.; Steiner, U. E. *J. Am. Chem. Soc.* **1999**, *121*, 1076–1087.
(67) Larson, S. L.; Elliott, C. M.; Kelley, D. F. *J. Phys. Chem.* **1995**, *99*, 6530–6539.
(68) Ott, S.; Borgström, M.; Hammarström, L.; Johansson, O. *Dalton Trans.* **2006**, 1434–1443.
(69) Wang, J.; Hanan, G. S.; Loiseau, F.; Campagna, S. *Chem. Commun.* **2004**, 2068–2069.
(70) Odobel, F.; Zabri, H. *Inorg. Chem.* **2005**, *44*, 5600–5611.
(71) Handa, S.; Wietasch, H.; Thelakkat, M.; Durrant, J. R.; Haque, S. A. *Chem. Commun.* **2007**, 1725–1727.
(72) Encinas, S.; Flamigni, L.; Barigelletti, F.; Constable, E. C.; Housecroft, C. E.; Schofield, E. R.; Figgemeier, E.; Fenske, D.; Neuburger, M.; Vos, J. G.; Zehnder, M. *Chem.—Eur. J.* **2002**, *8*, 137–150.
(73) Farley, S. J.; Rochester, D. L.; Thompson, A. L.; Howard, J. A. K.; Williams, J. A. G. *Inorg. Chem.* **2005**, *44*, 9690–9703.
(74) Graber, S.; Doyle, K.; Neuburger, M.; Housecroft, C. E.; Constable, E. C.; Costa, R. D.; Orti, E.; Repetto, D.; Bolink, H. J. *J. Am. Chem. Soc.* **2008**, *130*, 14944–14945.
(75) Beley, M.; Delabouglise, D.; Houppy, G.; Husson, J.; Petit, J. P. *Inorg. Chim. Acta* **2005**, *358*, 3075–3083.
(76) Lopez, R.; Villagra, D.; Ferraudi, G.; Moya, S. A.; Guerrero, J. *Inorg. Chim. Acta* **2004**, *357*, 3525–3531.
(77) Medina, A.; Claessens, C. G.; Rahman, G. M. A.; Lamsabhi, A. M.; Mo, O.; Yanez, M.; Guldi, D. M.; Torres, T. *Chem. Commun.* **2008**, 1759–1761.
(78) Anemian, R.; Cupertino, D. C.; Mackie, P. R.; Yeates, S. G. *Tetrahedron Lett.* **2005**, *46*, 6717–6721.
(79) Amthor, S.; Lambert, C. *J. Phys. Chem. A* **2006**, *110*, 1177–1189.
(80) Zbinden, K. G.; Obst-Sander, U.; Hilpert, K.; Kuhne, H.; Banner, D. W.; Bohm, H. J.; Stahl, M.; Ackermann, J.; Alig, L.; Weber, L.; Wessel, H. P.; Riederer, M. A.; Tschopp, T. B.; Lave, T. *Bioorg. Med. Chem. Lett.* **2005**, *15*, 5344–5352.
(81) Nazeeruddin, M. K.; Péchy, P.; Renouard, T.; Zakeeruddin, S. M.; Humphry-Baker, R.; Comte, P.; Liska, P.; Cevey, L.; Costa, E.; Shklover, V.; Spiccia, L.; Deacon, G. B.; Bignozzi, C. A.; Grätzel, M. *J. Am. Chem. Soc.* **2001**, *123*, 1613–1624.
(82) Becke, A. D. *Phys. Rev. A: Gen. Phys.* **1988**, *38*, 3098–3100.
(83) Becke, A. D. *J. Chem. Phys.* **1993**, *98*, 5648–5652.
(84) Lee, C.; Yang, W.; Parr, R. G. *Phys. Rev. B: Condens. Matter* **1988**, *37*, 785–789.
(85) Miehlich, B.; Savin, A.; Stoll, H.; Preuss, H. *Chem. Phys. Lett.* **1989**, *157*, 200–206.
(86) Dunning, T. H.; Hay, P. J. In *Modern Theoretical Chemistry*; Schaefer, H. F., III, Ed.; Plenum Press: New York, 1977; Vol. 3, pp 1−27.
(87) Hay, P. J.; Wadt, W. R. *J. Chem. Phys.* **1985**, *82*, 270–283.
(88) Hay, P. J.; Wadt, W. R. *J. Chem. Phys.* **1985**, *82*, 299–310.
(89) Wadt, W. R.; Hay, P. J. *J. Chem. Phys.* **1985**, *82*, 284–298.
(90) Frisch, M. J. et al. *Gaussian 03*, revision c.02; Gaussian Inc.: Wallingford, CT, 2004.
(91) These studies were carried out during the global MeCN shortage; thus, certain data is reported in other solvents.
(92) A TD-DFT analysis of all of the title complexes is not trivial and beyond the scope of this article. A more extensive computation treatise will be reported in a future study.
(93) A shortcoming in our DFT data is the prediction that the HOMO is localized predominantly to the TPA unit for all of the complexes (Supporting Information, Figures S5 and S6), which is not aligned with experimental data clearly showing that the HOMO is metal-based in certain cases.
(94) In our hands, a tpy ligand bearing a single $-CO_2H$ group is not effective for binding our TPA-substituted dyes effectively to TiO_2.
(95) Thermodynamic positions are based on the data for the respective methyl ester derivatives **3**, **10**, and **14**.
(96) Mishra, A.; Fischer, M. K. R.; Bauerle, P. *Angew. Chem., Int. Ed.* **2009**, *48*, 2474–2499.
(97) Boschloo, G.; Hagfeldt, A. *Acc. Chem. Res.* **2009**, *42*, 1819–1826.
(98) Marinado, T.; Nonomura, K.; Nissfolk, J.; Karlsson, M. K.; Hagberg, D. P.; Sun, L. C.; Mori, S.; Hagfeldt, A. *Langmuir* **2010**, *26*, 2592–2598.